Investigation of past earthquakes on the Titri Fault, coastal Otago, New Zealand

DJA Barrell
N Wang
MW Stirling
NJ Litchfield
BI Taylor-Silva
RJ Van Dissen
S Hornblow

GNS Science Report 2017/35
October 2020

DISCLAIMER

The Institute of Geological and Nuclear Sciences Limited (GNS Science) and its funders give no warranties of any kind concerning the accuracy, completeness, timeliness or fitness for purpose of the contents of this report. GNS Science accepts no responsibility for any actions taken based on, or reliance placed on the contents of this report and GNS Science and its funders exclude to the full extent permitted by law liability for any loss, damage or expense, direct or indirect, and however caused, whether through negligence or otherwise, resulting from any person's or organisation's use of, or reliance on, the contents of this report.

BIBLIOGRAPHIC REFERENCE

Barrell DJA, Litchfield NJ, Van Dissen RJ, Wang N, Taylor-Silva BI, Hornblow S, Stirling MW. 2020. Investigation of past earthquakes on the Titri Fault, coastal Otago, New Zealand. Lower Hutt (NZ): GNS Science. 66 p. (GNS Science report; 2017/35). doi:10.21420/G2TW6S.

DJA Barrell, GNS Science, Private Bag 1930, Dunedin 9054, New Zealand

NJ Litchfield, RJ Van Dissen, GNS Science, PO Box 30368, Lower Hutt 5040, New Zealand

N Wang, School of Geography, Environment and Earth Sciences, Victoria University of Wellington, PO Box 600, Wellington 6140, New Zealand

BI Taylor-Silva, Aurecon, PO Box 2292, Tauranga 3140, New Zealand

S Hornblow, Otago Regional Council, Private Bag 1954, Dunedin 9054, New Zealand

MW Stirling, Geology Department, University of Otago, PO Box 56, Dunedin 9054, New Zealand

ISSN 2350-3424 (online)
ISBN 978-1-98- 853016-1 (online)
http://dx.doi.org/10.21420/G2TW6S

CONTENTS

NON-TECHNICAL SUMMARY .... **III**

TECHNICAL ABSTRACT .... **IV**

KEYWORDS .... **IV**

1.0 INTRODUCTION **1**

1.1 Background 1
1.2 This Project 3

2.0 METHODS **4**

2.1 Trenching and Logging 4
2.2 Sampling and Dating 4
2.3 Documentation 5

3.0 TRENCH RESULTS **7**

3.1 Glenledi Road (trench T16/01) 7
3.1.1 Assessment of fault deformation 13
3.1.2 Assessment of timing of deformation events 18
3.2 Clarendon (trenches T16/02 and T16/03) 20
3.2.1 Excavation sequence 20
3.2.2 Trench T16/03 23
3.2.3 Trench T16/02 33

4.0 TITRI FAULT SURFACE RUPTURE CHARACTERISATION **43**

4.1 Chronology of Surface Rupture Events 43
4.2 Recurrence Interval 45
4.3 Single Event Displacement 45
4.4 Slip Rate 46

5.0 DISCUSSION **47**

5.1 Comparison with Previous Studies and Nearby Sites 47
5.2 Episodicity and Earthquake Clustering 47
5.3 Implications for Seismic Hazard Modelling 48

6.0 CONCLUSIONS **51**

7.0 ACKNOWLEDGMENTS **52**

8.0 REFERENCES **52**

FIGURES

Figure 1.1 Location map showing regional geology of the study area 2

Figure 1.2 A view looking southwest along the topographic step, up to the left (southeast), that runs across an alluvial fan at the Clarendon trenching site 3

Figure 2.1 Key to colours, patterns and linework used on the trench logs 6

Figure 3.1 Location map and landform interpretation for the Glenledi Road trench site, Titri Fault 7
Figure 3.2 Views of the Glenledi Road trench locality 8
Figure 3.3 Log of Trench T16/01, south-western wall...9
Figure 3.4 Log of Trench T16/01, north-eastern wall...10
Figure 3.5 Excavation of the Glenledi Road trench T16/01 13
Figure 3.6 Views of trench T16/01, Glenledi Road 14
Figure 3.7 The Titri Fault exposed in trench T16/01 15
Figure 3.8 Geological features illustrating the number and size of fault ruptures in trench T16/01 16
Figure 3.9 Samples for dating from Glenledi Road trench T16/01..19
Figure 3.10 Location map and landform interpretation for the Clarendon trench sites 21
Figure 3.11 Views of the Clarendon trenching locality...22
Figure 3.12 Views of trench T16/02 in early April 2016, prior to its extension in late April 2016....................23
Figure 3.13 Views of trench T16/03 during gridding and logging...24
Figure 3.14 Log of Trench T16/03, south-western wall...27
Figure 3.15 Log of Trench T16/03, north-eastern wall...28
Figure 3.16 Views of fault-deformation features in trench T16/03 31
Figure 3.17 Views of trench T16/03, showing fault-deformation features and sample locations 32
Figure 3.18 Views of the extension of trench T16/02...34
Figure 3.19 Views of the fault deformation in trench T16/02 35
Figure 3.20 Log of Trench T16/02, north-eastern wall, sheet 1 37
Figure 3.21 Log of Trench T16/02, north-eastern wall, sheet 2 38
Figure 3.22 Log of Trench T16/02, south-western wall..39
Figure 3.23 Views of sample sites in trench T16/02 42
Figure 4.1 OSL age constraints for the timing of rupture events on the Titri Fault from this study 44
Figure 5.1 Titri Fault segment sources for seismic hazard modelling purposes. 49

TABLES

Table 3.1 Glenledi Road trench T16/01 fault displacement information 11
Table 3.2 Dating results for the Titri Fault trenches...20
Table 3.3 Clarendon trench T16/03 fault displacement information 29
Table 3.4 Clarendon trench T16/02 fault displacement information 40
Table 4.1 Summary of net single-event displacement estimated for each trench site. 45
Table 4.2 Net slip rates from displacements of the older age-constrained geological features in each trench. 46
Table 5.1 Titri Fault alternative fault rupture scenarios...50

APPENDICES

APPENDIX 1 OSL DATING REPORT 57
APPENDIX 2 RADIOCARBON DATING REPORT...66

NON-TECHNICAL SUMMARY

The Titri Fault, a major geological structure in coastal Otago, southwest of Dunedin, has uplifted the coastal hills between Dunedin and Balclutha. Previously, it was unclear whether the Titri Fault is active, by the criterion of whether it had ruptured in the last 125,000 years. Consequently, the fault was not included in previous earthquake-hazard modelling. This study, funded by the Earthquake Commission, used trenching and geological dating investigations to obtain information on the nature and history of the most recent, large-earthquake-generating, rupture(s) of the Titri Fault. The main aim was to improve the understanding of Dunedin's seismic hazard. A secondary aim was, if possible, to find out whether previous earthquake ruptures of the Titri Fault have occurred regularly or in bursts (clusters) separated by periods of inactivity.

The trenches were located across steps in the ground surface suspected to have been produced by previous earthquake-generating ruptures of the fault. The suspected fault scarps were on alluvial fan landforms, one at Glenledi Road near Milton (one trench) and at Clarendon (two trenches), between Milton and Waihola. All three trenches revealed geologically-young sediments deformed by faulting and buckling, with an up-thrusting direction from the southeast to the northwest. Sediments were dated by a technique called Optically Stimulated Luminescence, which measures the time since the sediments were last exposed to sunlight, assumed to be when they were deposited on the fans or fault scarps. Through dating faulted and un-faulted sediments the timings of past large and potentially damaging earthquakes were able to be determined.

Information from the trench exposures and dating provided evidence for at least the last two ground surface rupturing earthquakes. The last earthquake occurred sometime between 18,300 and 31,300 years ago and the previous one sometime between 27,500 and 37,900 years ago. There is also reasonable evidence for at least one earlier, though undated, earthquake, and doubtful evidence for a later earthquake. The average amount of movement on the fault in each of the three well-defined earthquakes was approximately 2.6 m. The average fault slip rate (average rate of movement of the fault spanning several earthquakes) is in the range of 0.1 to 0.2 millimetres per year, which is a relatively low rate. The average time between large earthquakes (recurrence interval) is relatively long, lying within a range of approximately 7,000 to 19,000 years, most likely towards the longer part of that range.

The results show that the Titri Fault is an active fault and therefore poses a potential earthquake hazard for the Dunedin to Balclutha area. A future large earthquake on the Titri Fault is likely to have a magnitude somewhere between 7.0 and 7.7 and will cause strong ground shaking through the region, landsliding and liquefaction at susceptible sites, and disruption of the ground at the fault with uplift of the southeast side. The results provide hints, but not definitive evidence, of clusters of earthquakes on the Titri Fault, which could be investigated further with additional dating.

TECHNICAL ABSTRACT

The Titri Fault is a major southeast-dipping reverse fault in coastal Otago, southwest of Dunedin. The fault is up to 90 km long and has uplifted the coastal hills between Dunedin and Balclutha. Activity on the Titri Fault was previously poorly constrained, and the fault has not previously been included in the New Zealand National Seismic Hazard Model (NSHM). Two suspected fault scarps were identified on alluvial fans along the Titri Fault and were investigated via an Earthquake Commission Biennial Contestable Grants Programme project. The aim of the project was to trench the scarps and obtain quantitative data on the nature and history of the most recent rupture(s) of the Titri Fault, in order to improve the understanding of Dunedin's seismic hazard. A secondary aim was to investigate whether ruptures of the Titri Fault have been clustered in time.

Three trenches were sited across the suspected surface fault scarps on alluvial fans that drain northwest onto the Taieri and Tokomairaro plains at Glenledi Road near Milton (one trench) and at Clarendon (two trenches). All three trenches exposed reverse faulted and folded Quaternary-age alluvial fan deposits and colluvial wedges, with near-surface fault dips ranging from 24° to 67° SE. Collection of samples for chronological analysis comprised 21 samples for optically stimulated luminescence (OSL) dating and five samples for radiocarbon dating; the budget allowed the dating of seven OSL samples and one radiocarbon sample.

Stratigraphic evidence for past surface ruptures of the Titri Fault was found in all three trenches. All trenches showed evidence for at least two surface ruptures, with suggestions of two more surface rupture events at the Glenledi Road trench site, one likely earlier event and one doubtful later event. Dating shows that the two most recent ruptures could have been the same in all three trenches. The most recent rupture was between 18.3 and 31.3 ka (1 ka = 1000 years before present) and the penultimate rupture was between 27.5 and 37.9 ka. Fault parameters quantified as a result of this study include single-event net displacements in the range of 2.4 to 2.7 m, average fault slip rate in the range of 0.1 to 0.2 mm/yr, and a poorly constrained recurrence interval range of ~7000 to 19,000 years, with a preferred value towards the longer end of that range. The results provide hints, but not definitive evidence, of episodic activity (clustered ruptures) on the Titri Fault.

The results demonstrate that the Titri Fault is an active fault with relatively low activity and should be included in future versions of the NSHM. In seismic hazard modelling, the Titri Fault has been represented as three ~30 km long segments with rupture of individual segments modelled as able to produce earthquakes of Mw ~7.0 and ruptures of two or all three segments generating earthquakes up to Mw ~7.7. Potential temporal clustering and refinement of plausible rupture scenarios could be tested through dating of remaining OSL samples collected from the Glenledi Road and Clarendon trenches, and through future trench investigations at other sites such as a prominent scarp near Moneymore.

KEYWORDS

Titri Fault, active fault, earthquake geology, Quaternary geology, geological dating, geological hazards, paleoseismology, Dunedin City, Otago, OSL dating.

1.0 INTRODUCTION

1.1 Background

The Titri Fault is a major geological structure in coastal Otago, southwest of Dunedin. Aligned northeast-southwest and dipping to the southeast, uplift on the south-eastern side of the fault has elevated a range of coastal hills, which separates the low-lying Taieri and Tokomairaro plains from the coast (Figure 1.1).

The Titri Fault has a complex geological history. On its now uplifted south-eastern side lies the Henley Breccia (Figure 1.1), an up to ~1 km thick deposit of breccia and conglomerate. Henley Breccia is interpreted to have been deposited in a fault-angle depression created by normal movement (down to the southeast) on the Titri Fault during the mid- to Late Cretaceous (sometime between ~112 and 85 Ma[1]) (Mutch and Wilson 1952). Other nearby structures, including the Castle Hill Fault and Tokomairiro Fault (Figure 1.1), were also involved in Late Cretaceous normal movement (Harrington 1958). Normal movement may have continued into the Early Cenozoic Era, because the Late Cretaceous to Eocene (~85 to ~35 Ma) sedimentary rock sequence (Figure 1.1; Haerenga Supergroup) southeast of the Titri Fault near Dunedin is markedly thicker (~700 m; McKellar 1990) than it is northwest of the fault, at the few localities where that sequence is preserved (< ~250 m; maps of Benson (1968) and Bishop (1994)).

A change in the regional tectonic regime from extension to contraction in the Late Cenozoic (younger than ~23 Ma) caused reversal of movement on the Titri Fault and raised its previously downthrown south-eastern side by as much as 500 m. A lack of obvious evidence for offset of Late Quaternary landforms along the line of the Titri Fault meant that the fault was not regarded as active on, for example, the Bishop (1994) and Bishop and Turnbull (1996) geological maps. It was, however, recognised that the fault movement had continued through to at least the Early or Middle Quaternary, because there are deposits of tectonically deformed fluvial gravel (Gladstone Road Gravel) close to the fault (McKellar 1990; Bishop 1994).

New information relevant to evaluating the possibility of ‘young’ displacements on the Titri Fault arose from research carried out in the late 1990s, comprising a mapping study of Quaternary river terraces and alluvial fans of coastal Otago (Barrell et al. 1998, 1999), and a University of Otago doctoral thesis on active faulting in the coastal Otago region (Litchfield 2000). Fieldwork and aerial photograph interpretation identified suspected surface fault traces (scarps) along the Titri Fault near Moneymore, between 4 and 7 km southwest of Milton (Barrell et al. 1998), and uplifted and back-tilted alluvial fan surfaces were identified along the central sector of the fault between Lake Waihola and Mosgiel (Litchfield 2000). At that time, no funds were available for detailed paleoseismic investigations of the fault’s activity, such as by trenching, and this prevented a quantitative chronology being placed on the Titri Fault’s most recent movements. Litchfield (2001) inferred, on geomorphic grounds, that the most recent movement on the Titri Fault occurred during the middle of the Last Glaciation, which spanned from ~18-74 ka[2]. However, Optically Stimulated Luminescence (OSL) dating of loess associated with alluvial fans was later reported by Litchfield and Lian (2004) and interpreted to indicate that no movement of the Titri Fault had occurred since ~92 ka.

[1] 1 Ma = 1 million years before present

[2] 1 ka = 1000 years before present

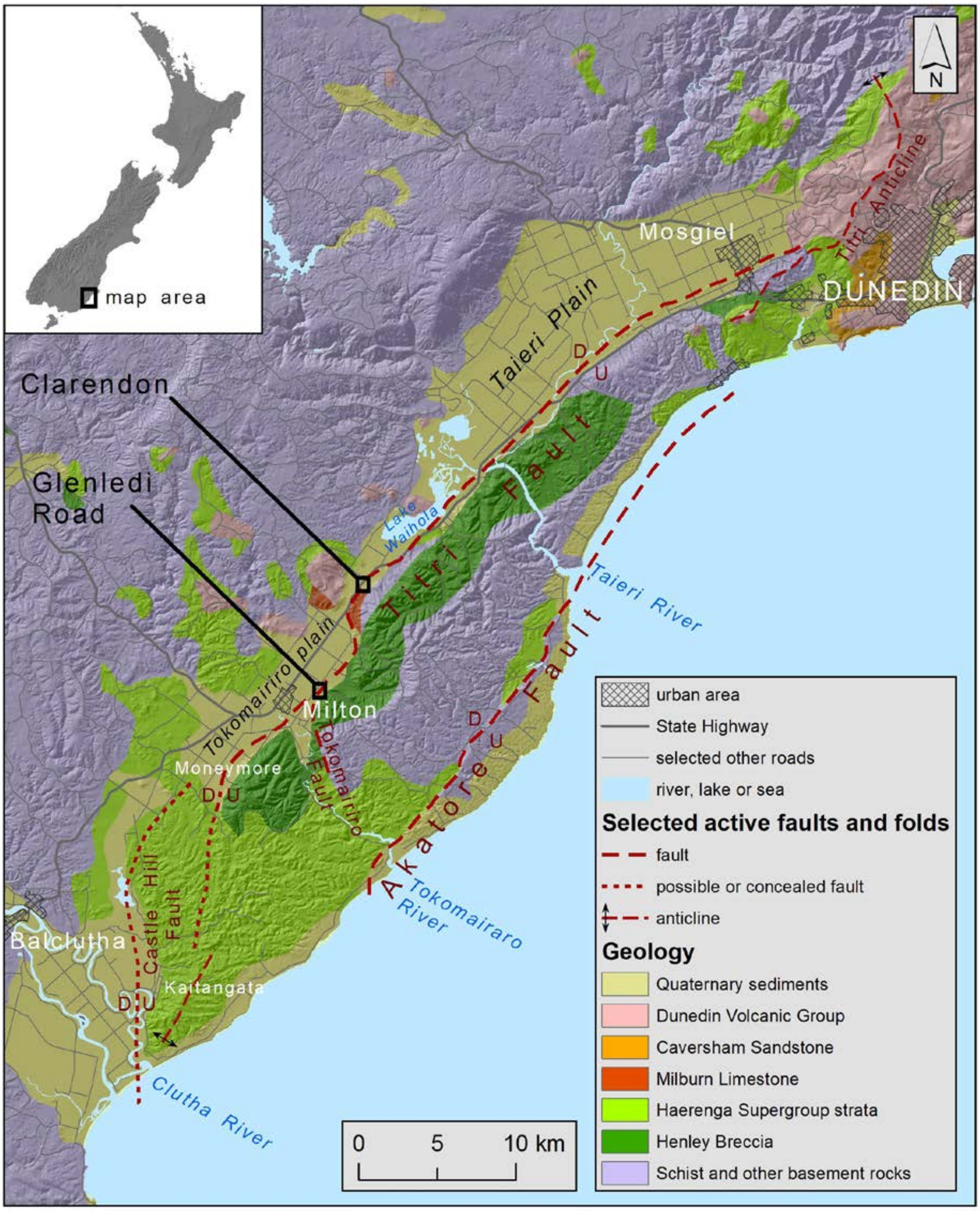

Figure 1.1 Location map showing regional geology of the study area (from Edbrooke et al. 2014), the Titri Fault (and associated structures), the Akatore Fault, and the Glenledi Road and Clarendon trenching localities.

Geologically-recent surface rupture scarps were recognised on the nearby northeast-southwest striking Akatore Fault during the 1960s, leading to it being classified as active (Litchfield and Norris 2000). Based on the information obtained in the late 1990s, the Titri Fault was reclassified as an active fault in the 1:250,000-scale Geological Map of New Zealand (QMAP) database (Heron 2018). The Titri Fault is now included in the New Zealand Active Faults Database (https://data.gns.cri.nz/af/; Langridge et al. 2016), but of the coastal Otago faults, only the Akatore Fault is currently designated as an active fault earthquake source in the New Zealand National Seismic Hazard Model (Stirling et al. 2012).

1.2 This Project

Several years ago, one of us (Barrell) noticed landform features possibly formed during the most recent movement(s) of the Titri Fault at two sites, one near the rural locality of Clarendon, and one close to Glenledi Road near Milton township (Figures 1.1 and 1.2). The landform features comprise small steps on alluvial fan terraces. The steps are up to the southeast, at approximately the projected location of the fault. In these general areas the fault position is somewhat uncertain because there are few outcrops of bedrock to define its structural location. This meant that subsurface investigations would be necessary to assess whether the landform features are fault-related. In the eastern South Island, a long-standing difficulty in defining chronologies for recent active fault movements is that organic materials that are suitable for radiocarbon dating are rarely preserved in sedimentary deposits, due to the relatively dry climate. This has been overcome in the past 20 years or so by continued success in the application of OSL dating, for example in the Waitaki valley in the central South Island (Barrell et al. 2009).

Deposits of fine sand or silt suitable for OSL dating are very common throughout the eastern South Island, providing heightened confidence that a focused investigation of the most recent movements of the Titri Fault would yield useful dating results. Following a successful application to the Earthquake Commission Biennial Contestable Grants Programme, we commenced investigations on the Titri Fault in the late summer of 2016. The aim of this project was to obtain quantitative data on the nature and history of the most recent rupture(s) of the Titri Fault, in order to improve the understanding of Dunedin's seismic hazard. A secondary aim, contingent upon what the trenching and dating found, was to investigate whether ruptures of the Titri Fault have been clustered in time, similar to what has been interpreted for other active faults in Otago, such as the Akatore Fault (Litchfield and Norris 2000; Taylor-Silva et al. 2020) and the Pisa Fault (Beanland and Berryman 1989). This report presents the results of the 2016 Titri Fault paleoseismic trenching investigations.

Figure 1.2 A view looking southwest along the topographic step, up to the left (southeast), that runs across an alluvial fan at the Clarendon trenching site. The step was suspected to have been formed by movement of the Titri Fault. Trench T16/03 was subsequently excavated across this step and confirmed its fault origin. Photo: GNS Science, N.J. Litchfield.

2.0 METHODS

2.1 Trenching and Logging

Three investigation trenches were dug across the suspected scarps of the Titri Fault using a 12-tonne excavator, following GNS Science standard procedures – one at the Glenledi Road site, and two at the Clarendon site (Figure 1.1). First, the team inspected each site and decided upon the best location for commencing excavation. Trench design comprised a ~6–7 m wide footprint. Topsoil was stockpiled for later restoration and the footprint was excavated to a depth of about 2 m. A central slot about 2 m wide and 2 m deep was then excavated on the initial floor of the trench to provide a benched geometry in which it was safe for people to work. Trenches were excavated to sufficient length to achieve geological objectives, e.g. satisfactory exposure of fault-deformed deposits in the trench walls and sufficient distance either side of the fault to see and understand the un-faulted deposit stratigraphy.

Trench walls were cleaned using hand scrapers and brushes to provide clear exposure of the geological materials and the team selected which wall, or parts of walls, would be logged. A one-metre grid of horizontal and vertical string lines was affixed to each logging wall using a tripod-mounted survey level, stadia staff and tape measures, and reference meterages were marked up with spray paint. The reference meterages are specific to each trench, and the height axes are relative to the trench site, not elevation above sea level, for example. The 0-m height line approximates the highest ground surface level at the trench, and where both trench walls were logged, the same height grid values are used in both walls.

Geological features, such as fault planes and boundaries between sediment layers, were recorded by a team of two geologists (the measurer and the recorder), on a scale drawing (log) made on large (A2 size) sheets of graph paper at 1:20 scale. A hand-held tape was used to measure coordinate positions of each geological feature relative to the metre gridlines. In most cases, the initial geological interpretations evolved during logging, as the geologists became more familiar with the features of the trenches and began to identify subtleties that were not initially apparent. An important component of the logging work was on-site peer review of the trench logs, carried out by a team member or members who were not involved in the preparation of that specific log.

The walls were photographed multiple times during the work, first after the completion of excavation and cleaning, second after the completion of gridding and third after the completion of logging and sample collecting. Multiple photography safeguards against a loss of information, for example, should part of a trench wall collapse after excavation or if a rainstorm were to wash mud down the trench walls and obscure the geological features.

Following the completion of work, the trenches were backfilled, and topsoil restored.

2.2 Sampling and Dating

Two dating methods were employed for this project, radiocarbon and OSL dating. OSL dating is a mainstay for young geological deposits in Otago because the organic sub-fossil remains (e.g. wood, charcoal etc) necessary for radiocarbon dating are less commonly present than the sandy or silty layers which are suitable for OSL dating. As it turned out, several samples potentially suitable for radiocarbon dating were collected as part of this project, but most of the samples collected were for the purposes of OSL dating.

OSL dating samples were collected by driving steel tubes into the target sediment layer, and then digging out the tube and sealing it either end using aluminium foil, tape and black plastic. Prior to driving the tube, the trench wall at the sample site was excavated back between 10 and 30 cm, to provide a fresh face that had minimal exposure to daylight. Different depths reflected the nature of the sample site; lesser excavation was used for thin silt layers or silt pods in gravel. Samples were labelled and stored at the GNS Science Dunedin Research Centre. Seven samples were selected for dating, and this was performed at the Luminescence Dating Laboratory at Victoria University of Wellington (Appendix 1).

Samples for radiocarbon dating were excavated from the trench wall either as block samples in the case of organic layers or as loose fragments in the case of charcoal flecks or twig-like materials. Samples were sealed in plastic bags, labelled and stored at the GNS Science Dunedin Research Centre. Only one radiocarbon sample was selected for dating, and this was undertaken at the Rafter Radiocarbon Laboratory in Lower Hutt (Appendix 2).

2.3 Documentation

The trench log sheets were scanned at high resolution and digitised using ArcGIS software. A general key to the trench log symbology is presented in Figure 2.1, and detailed descriptions are provided on each log sheet. Our approach uses colours and patterns to convey the nature and/or origin of the geological materials, while a number and letter code is used on each log to link with a material description on the log face. The numbering system conveys information about the relative amount of fault deformation that the geological sequence exposed in each trench has undergone and is specific to each trench. There are five groups of units, with generally increasing age. Group 1 comprises topsoil materials, and group 2 denotes geological strata that are interpreted to have not been deformed by fault movement (i.e. were deposited after the most recent movement). Group 3 represents strata that have experienced some fault deformation after they were deposited, while group 4 encompasses strata that are more deformed than those of group 3 (i.e. have experienced more than one fault deformation event). Group 5 strata denote even older geological materials and, in the case of this project, represent bedrock. The letter code accompanying the number broadly represents the age sequence, for example letter ‘a’ usually represents the youngest stratum of the group, and sequential letters broadly represent progressively older strata. This however is not ubiquitous, and the main purpose of the letter code is to link to a specific description. The letter codes are specific to each trench.

The sizes of fault offsets discussed in this report were measured off the trench logs, either along the faults (net slip) or by the vertical separation of units across the faults (vertical offset). Dating results are provided in reports from the laboratories and are appended to this report (Appendix 1 – OSL dating; Appendix 2 – Radiocarbon dating). In the information obtained from the trenching, there was no evidence that could be used to determine whether or not there was any strike-slip component of movement. Therefore, all the interpretations of fault movement assume that movement has been entirely dip-slip.

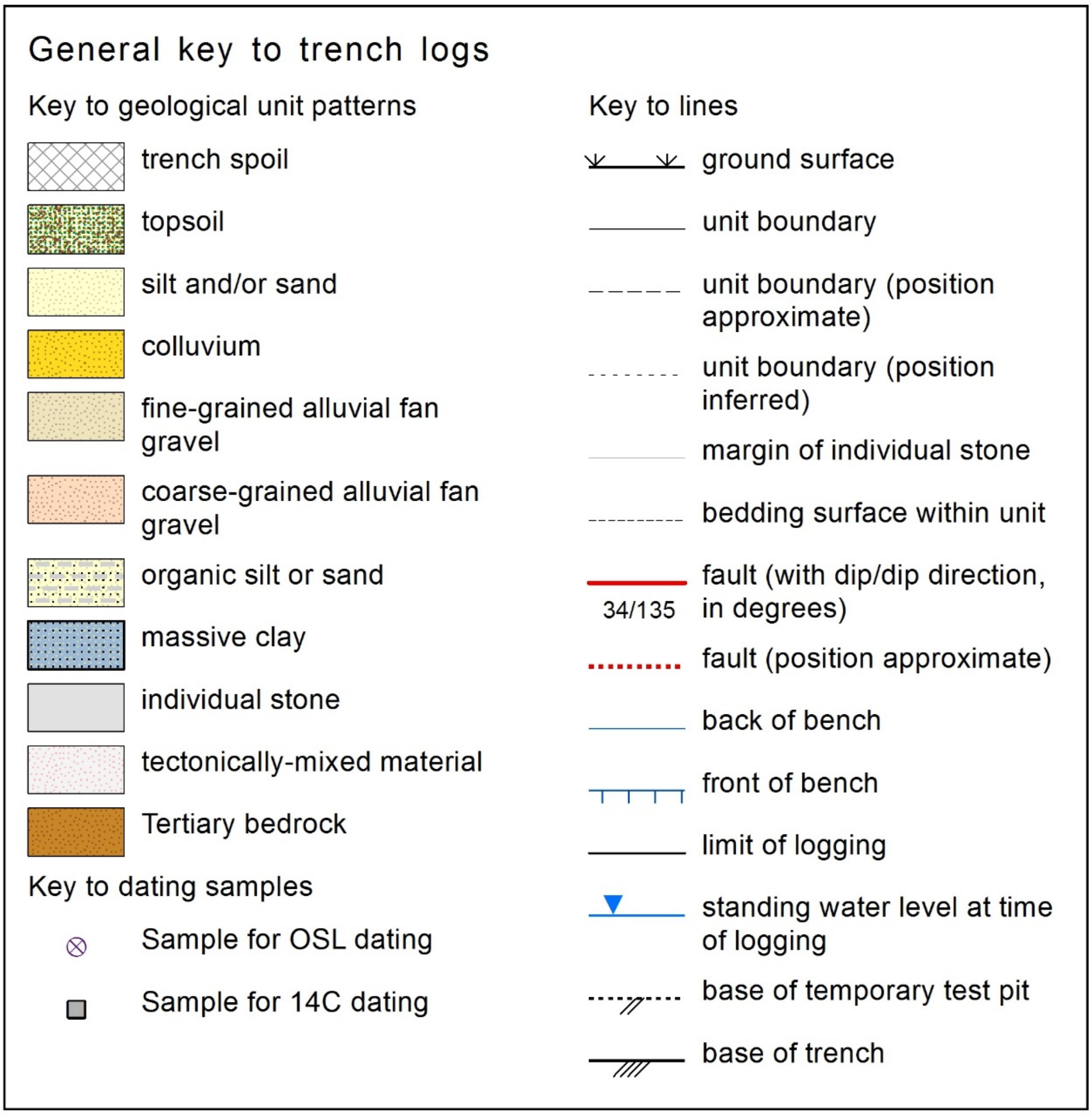

NOTE: Individual units in trenches are labelled with a number and a letter (e.g. 2a). Numbers 1 and 2 indicate that the unit is younger than the most recent fault deformation. Number 3 indicates that the unit has experienced some deformation, while units 4 and higher have experienced progressively greater amounts of deformation. The letters are sequential and provide a link to a material description on the log face. The numbering/lettering system is specific to each trench, so for example unit 3d in one trench may be a different material to 3d in another trench. The same number/letter coding applies to both walls within a single trench.

Figure 2.1 Key to colours, patterns and linework used on the trench logs. 14C dating refers to the radiocarbon method.

3.0 TRENCH RESULTS

3.1 Glenledi Road (trench T16/01)

The Glenledi Road trench site lies about 3 km east of Milton, on the north-western edge of a small 'island' on the alluvial fan plain of Salmonds Creek (Figures 3.1 and 3.2). Prior to trenching, this island was interpreted to be a remnant of fault-uplifted alluvial fan, which had escaped being eroded away by the action of the creek subsequent to the faulting movement(s).

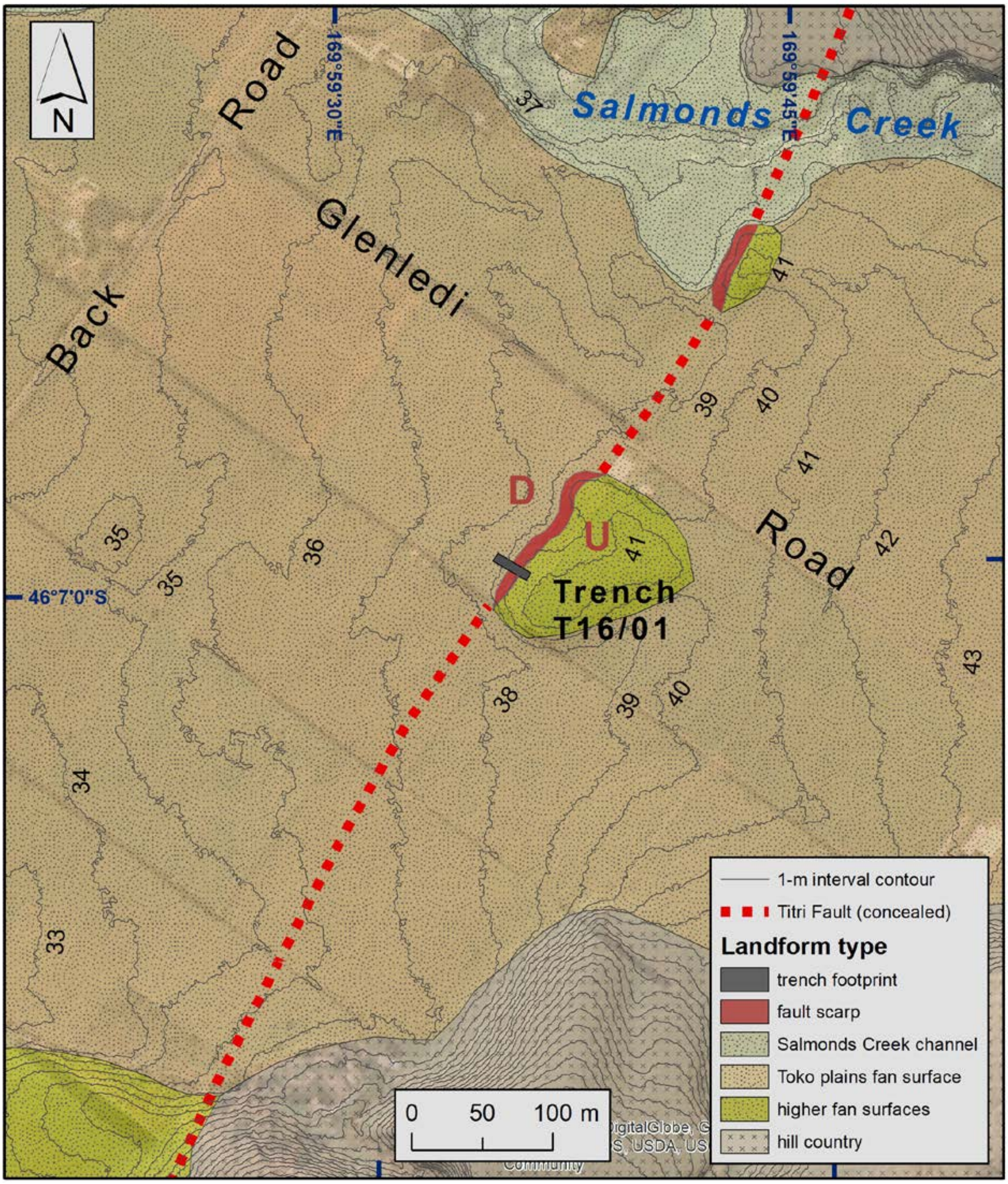

Figure 3.1 Location map and landform interpretation for the Glenledi Road trench site, Titri Fault. The topographic contours (metres above sea level) were generated from an Otago Regional Council lidar digital elevation model (DEM) and highlight the ~100 m by 100 m 'island' remnant of fault-uplifted alluvial fan that has escaped erosion by Salmonds Creek. A similar smaller remnant lies alongside the creek to the north. The background aerial photo is from the ArcGIS basemap layer.

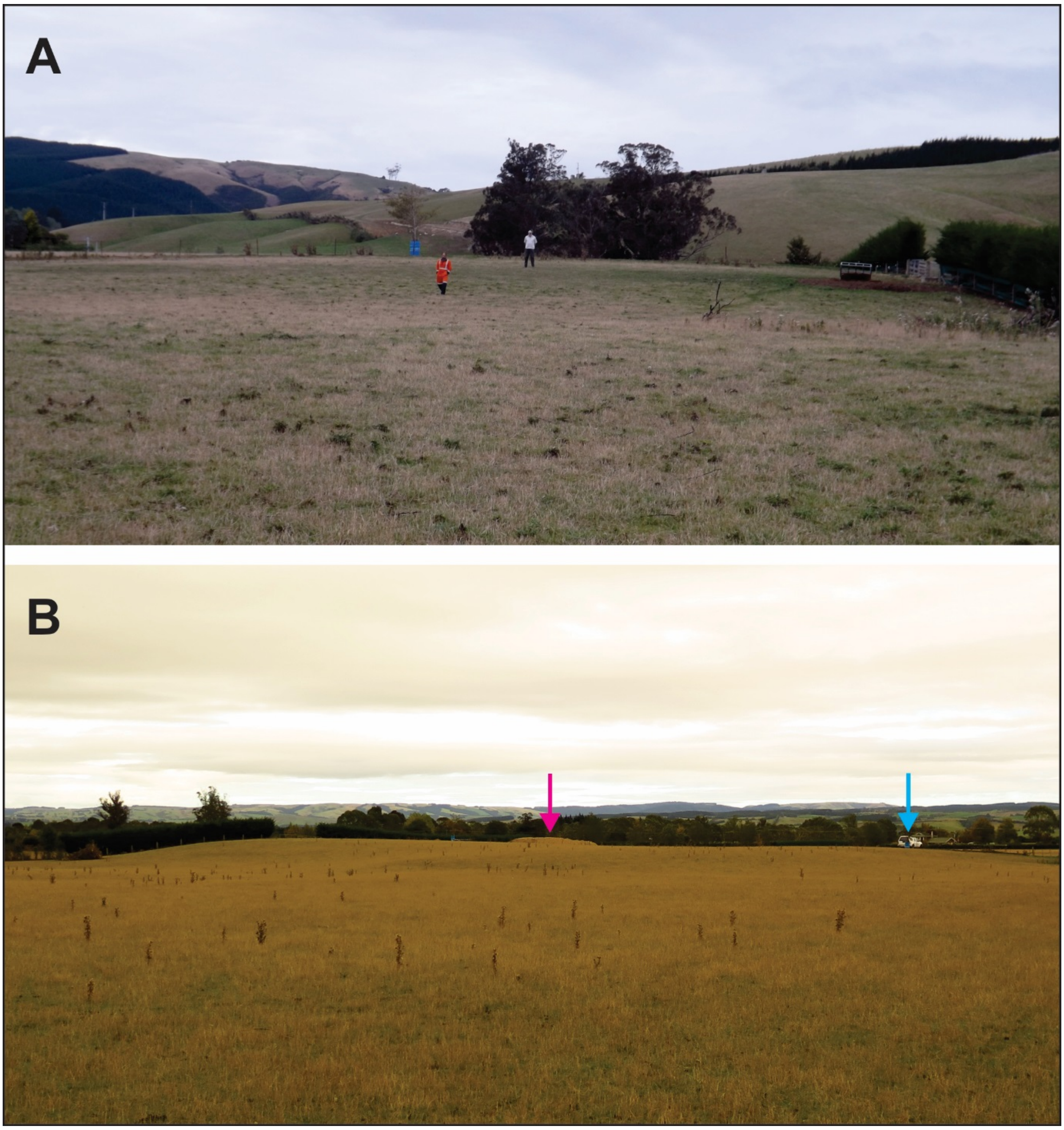

Figure 3.2 Views of the Glenledi Road trench locality. A: The topographic step that was confirmed by trenching to be a fault scarp, looking southeast. Trench T16/01 was excavated near where the people are standing. Photo: GNS Science, N.J. Litchfield. B: Looking northwest towards the alluvial fan 'island', which is a remnant of ground uplifted by Titri Fault ruptures. Arrowed are the trench T16/01 spoil pile (pink) and a vehicle (blue). Photo: GNS Science, D.J.A Barrell.

The trench successfully uncovered sediments offset by rupture(s) of the Titri Fault. The trench (Figures 3.3, 3.4, and 3.5) exposed alluvial fan gravels, with minor lenses of sand and silt, deposited by Salmonds Creek (unit group 4) resting on a stream-eroded surface cut on weathered sandstone/claystone bedrock (unit 5). This bedrock unit is likely to be Abbotsford Formation, of Paleogene age (~66–34 Ma), which Bishop (1994) maps on the downthrown side of the fault north of Salmonds Creek. The trench exposure shows that the base of the alluvial fan deposits is about 5 m higher on the south-eastern (upthrown) side of the fault (Figures 3.3, 3.4, and 3.6). Gravelly silt (unit 3) is draped and faulted across the fault scarp and adjoins a sequence of silt and gravelly silt on the north-western, downthrown, side of the fault (unit groups 2 and 3) (Figure 3.7 and 3.8). Fault displacement information from the trench exposure is collated in Table 3.1. Deposition of unit group 2 sediments and formation of unit 1 topsoil are interpreted to have occurred after the most recent fault deformation at this site.

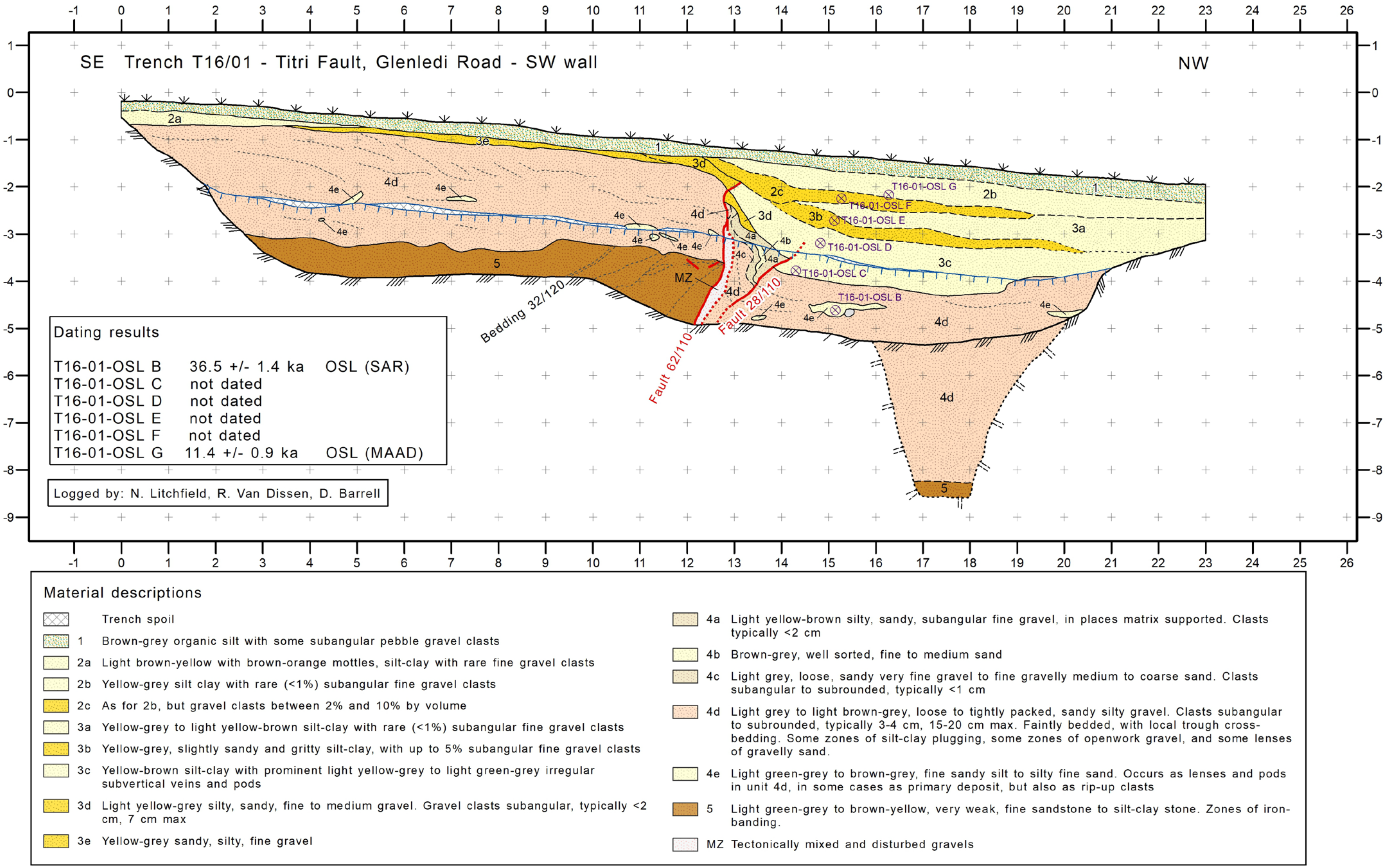

Figure 3.3 Log of Trench T16/01, south-western wall. Log axes are in metres. The fault attitudes are field measurements and differ from the representative fault-dip values given in Table 3.1 and discussed in the text. Minor discontinuous units within a more extensive unit are labelled in smaller font. More information on the dating samples and results is presented in Table 3.2.

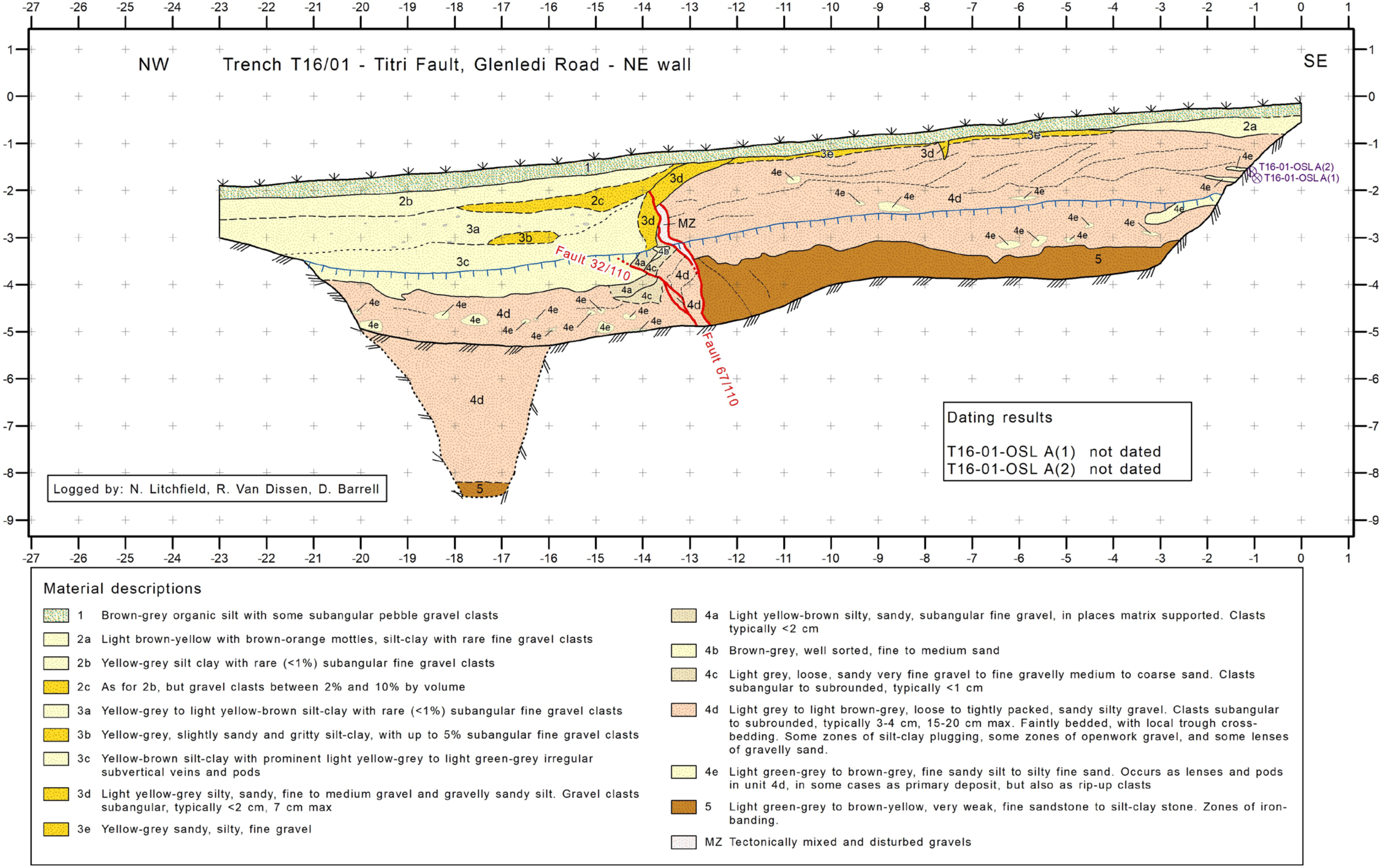

Figure 3.4 Log of Trench T16/01, north-eastern wall. Log axes are in metres. The fault attitudes are field measurements and differ from the representative fault dip values given in Table 3.1 and discussed in the text. Minor discontinuous units within a more extensive unit are labelled in smaller font. The dating samples were collected from a lens of unit 4e in the back wall of the trench.

Table 3.1 Glenledi Road trench T16/01 fault displacement information. The values have been estimated from the trench logs (Figures 3.3 and 3.4). Fault dip values differ from fault attitudes on the logs that were measured in the field on localised sectors of the fault planes.

<table>
<tr><th rowspan="2">Geological Feature</th><th colspan="3">Fault Dip (degrees)</th><th colspan="3">Vertical Separation (m)</th><th colspan="3">Dip-slip Displacement (m)</th><th rowspan="2">Estimated Number of Surface-Rupture Events</th><th colspan="2">Average Dip-Slip Single-Event Displacement (m)</th></tr>
<tr><th>average</th><th>minimum</th><th>maximum</th><th>median</th><th>minimum</th><th>maximum</th><th>average</th><th>minimum</th><th>maximum</th><th>minimum</th><th>maximum</th></tr>
<tr><td>Contact between top of unit 5 (bedrock) and base of unit 4d (overlying alluvial fan gravel) either side of the fault zone</td><td rowspan="3">57°</td><td rowspan="3">40°</td><td rowspan="3">73°</td><td>5.0</td><td>4.8</td><td>5.2</td><td>6.0</td><td>5.0</td><td>8.1</td><td>At least 3 and possibly at least 4</td><td>1.3</td><td>2.7</td></tr>
<tr><td>Difference in thickness of unit 4 (alluvial fan gravel package) either side of the fault zone</td><td>1.8</td><td>1.5</td><td>2.0</td><td>2.1</td><td>1.6</td><td>3.1</td><td>At least 1</td><td>-</td><td>3.1</td></tr>
<tr><td>Contact between top of unit 4 (alluvial fan gravel package) and the base of unit 3 (silt and gravelly silt package) either side of the fault zone</td><td>3.3</td><td>3.0</td><td>3.6</td><td>3.9</td><td>3.1</td><td>5.6</td><td>At least 2 and possibly at least 3</td><td>1.0</td><td>2.8</td></tr>
<tr><td>Difference in height of base of unit 3d (colluvial gravel and gravelly silt) within the fault zone</td><td>-</td><td>-</td><td>73°</td><td>-</td><td>1.0</td><td>-</td><td>-</td><td>1.0</td><td>-</td><td>At least 2 and possibly at least 3</td><td>0.3</td><td>-</td></tr>
</table>

NOTES

Fault dip values were estimated from the logs using a protractor. Four representative estimates were taken over the basal one metre of the logged trench wall, one each on the north-western and south-eastern sides of the fault zone, in each wall. The maximum dip is the steepest value, the minimum dip is the gentlest value, and the average is of all four values. These fault dip values are applied to the vertical separations of each of the geological features listed in the table, irrespective of what localised dip(s) the fault(s) may have at the location of the feature.

Vertical separation of each geological feature across the fault zone is taken from the logs, and includes representative estimates of maximum and minimum separation, based on plausible options for projection of each geological feature into the fault zone (see text for additional information). The median value is midway between the minimum and maximum. The thickness difference in unit 4 either side of the fault is, strictly speaking, not a vertical separation.

Dip-slip displacement is calculated from the fault dip and vertical separation. The average value is based on the average fault dip and median vertical separation, the maximum value uses the maximum fault dip and minimum separation, and the minimum value comes from maximum fault dip and minimum vertical separation.

The estimated numbers of single-event displacement events refer to the number of surface ruptures that produced the vertical separation of each geological feature.

The dip-slip single-event displacement is the dip-slip displacement value divided by the number of single-event displacements. The minimum value is based on the minimum displacement and larger estimate of events, while the maximum value comes from the maximum displacement and smaller estimate of events.

This page left intentionally blank.

3.1.1 Assessment of fault deformation

A reverse sense of displacement is confirmed by upthrow to the southeast on a moderate to steeply south-easterly dipping fault zone, up to 2 m wide and containing multiple fault planes. Fault planes on the south-eastern side of the fault zone (Figure 3.7B) dip more steeply than those on north-western side (Figure 3.8B). The north-western side of the fault zone has overall fault plane dips of 40° (south-western wall) and 52° (north-eastern wall), while the south-eastern side of the fault zone has overall fault plane dips of 64° (south-western wall) and 73° (north-eastern wall). Our adopted minimum, average and maximum fault dip values at the trench location are 40°, 57° and 73° respectively (Table 3.1).

Figure 3.5 Excavation of the Glenledi Road trench T16/01. A: A view northwest during excavation, following initial exposure of the fault. B: Geologists Barrell and Van Dissen make the first preliminary inspection of the newly exposed fault, with Tertiary bedrock (orange; unit 5) overlain by alluvial fan gravel (grey-brown; unit 4) faulted, up to the left, against alluvial fan gravel and silt (yellow-brown; units 3 and 2). C: The freshly-exposed fault offset in the north-eastern wall of the trench. Photos: GNS Science, N.J. Litchfield.

Figure 3.6 Views of trench T16/01, Glenledi Road. A: A northwest view of the digger excavating a temporary test pit into the trench floor on the downthrown side of the fault. At near-maximum reach, the digger managed to expose the orange Tertiary bedrock (unit 5, as exposed in foreground on the upthrown side of the fault) beneath alluvial fan gravel (unit 4) on the downthrown side of the fault. Photo: GNS Science, N.J. Litchfield. B: Looking northwest along the newly completed trench, after backfilling of the temporary test pit at the far end of the trench floor. Photo: GNS Science, D.J.A Barrell.

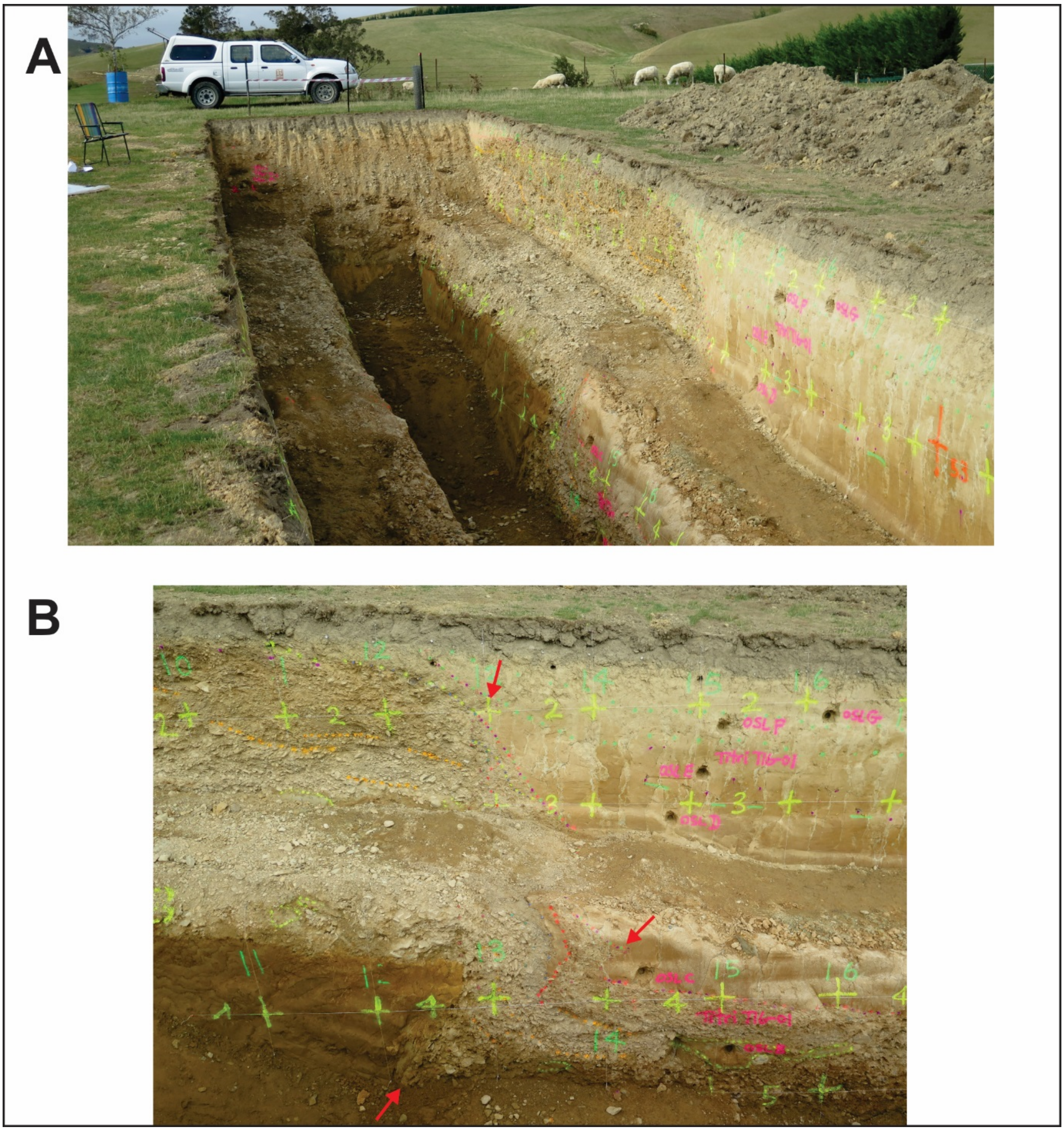

Figure 3.7 The Titri Fault exposed in trench T16/01. A: Southeast view of the trench after logging (string lines and yellow-painted 1-m grid crosses) and showing sample locations (pink paint). B: View of the south-western wall, showing the fault offset and deformation; red arrows highlight the ends of the exposed fault planes, with considerable buckling of sedimentary layers across the fault zone. The arrow right-of-centre marks the tip of the lower-angle splay fault. Both photos: GNS Science, D.J.A Barrell.

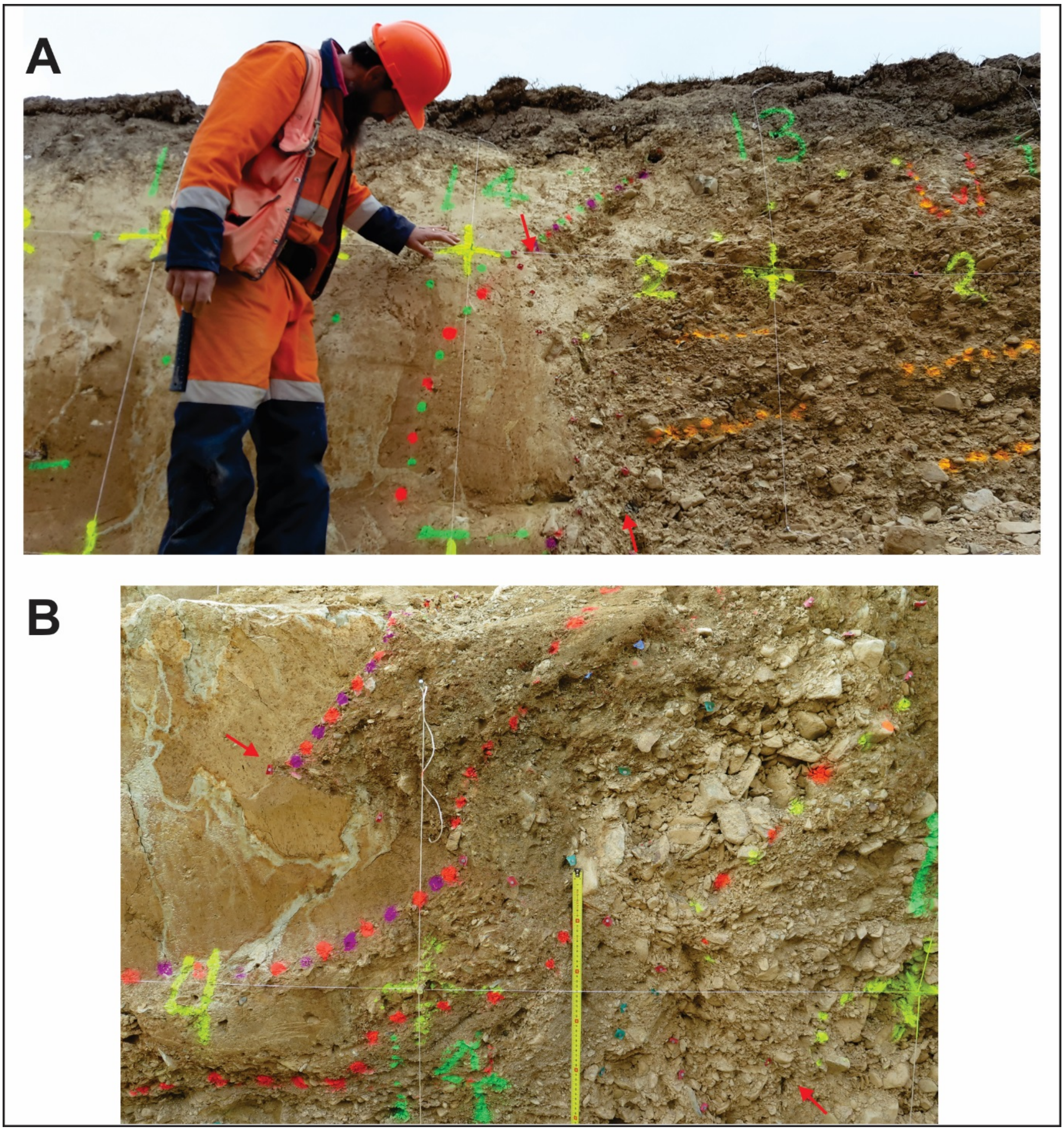

Figure 3.8 Geological features illustrating the number and size of fault ruptures in trench T16/01. A: This view of the north-eastern wall, meterage -15 to -12 horizontal, -1.5 to -3 vertical (Figure 3.4), shows unit 3d colluvium (right of the red/green dotted line), standing almost vertically against fault-disturbed gravel (MZ; approximately indicated by red arrows), with unit 4d alluvial fan gravel to the right, with orange paint indicating depositional boundaries within the gravel. At least two fault ruptures events are indicated here, one to disrupt the gravel and form a step over which unit 3d colluvium was deposited, and another to tilt unit 3d into a near-vertical orientation. Photo: GNS Science, R. Smillie. B: View of the north-eastern wall, meterage -14.5 to -13 horizontal, -3.0 to -4.25 vertical (Figure 3.4), The top of unit 4a (red/purple dots) and unit 4c (red dots) are offset, up to the right, across a lower-angle fault strand (red arrows) dipping 32 ° to the right (east-southeast). This ~40 cm of reverse offset is likely to represent a minimum value for single-event displacement. The tape is extended 50 cm. Photo: GNS Science, D.J.A Barrell.

We are confident that there are definitely at least two, probably at least three, and possibly at least four, fault rupture events recorded in the stratigraphy exposed in the trench. It is likely that the difference in thickness of the unit 4 sediment package either side of the fault represents the oldest rupture event, or events, recorded in the stratigraphy. The sediment package is between 1.5 and 2 m thicker on the downthrown side of the fault. One explanation for the thickness difference is that the unit 4 alluvial fan gravel package was deposited in its entirety, after which one or more rupture events raised the south-eastern side of the fault, and Salmonds Creek eroded a 1.5 to 2 m thickness of the alluvial fan sediments off the upthrown side, and carried the eroded materials downstream, away from the location that was trenched (option 1). Another explanation is that the lower part of unit 4 northwest of the fault is an older alluvial fan deposit, preserved northwest of the fault following a fault rupture. By this explanation, the stream planed off the bedrock southeast of the fault, and then deposited about 2.5 m of alluvial fan gravel on both sides of the fault, forming the entirety of unit 4 southeast of the fault, and the upper part of unit 4 northwest of the fault (option 2). A third possibility is that the stream may have originally cut localised deeper channels into the bedrock, with thicker gravels in those channels, and the test pit below the north-western part of the trench happened to encounter such a channel. We regard this as less likely than a fault-related origin for the thickness difference.

A subsequent rupture is interpreted to have uplifted the south-eastern side of the fault, forming a scarp in unit 4 alluvial fan sediments, with erosion of those sediments from the uplifted side forming a deposit of colluvial gravel (unit 3d) across the scarp (Figure 3.8A). These events were followed by enough time to deposit unit 3c.

At least one further rupture was necessary to have offset (Figure 3.3) or steeply buckled (Figures 3.4 and 3.8A) the unit 3d colluvium. This event likely resulted in deposition of colluvial unit 3b and was later followed by deposition of unit 3a.

A fourth possible event may have increased the elevation of the upthrown side of the fault, resulting in the deposition of colluvial unit 2c. The uplift and erosion due to this possible event may have eroded away colluvial unit 3b at the fault, and with it, any evidence for faulting of unit 3b. The lack of direct evidence, and because it is plausible that the partial erosion of unit 3b and deposition of unit 2c came about through non-faulting processes such as storm events, means this fourth rupture event is seen as a speculative and less likely possibility.

There is no evidence of fault displacement cutting or deforming the base of unit 2c and, accordingly, we regard the unit 2c deposit, and all overlying units, to definitely be younger than the most recent surface fault rupture at this site. It is possible, and perhaps likely, that deposition of units 3a and 3b also post-date the most recent surface rupture at this site.

Four geological features are considered sufficiently distinctive across the fault zone to provide useful estimates of amounts of fault displacements. They are listed in Table 3.1 and described below.

The first is the contact between the top of unit 5 (bedrock) and the base of unit 4 (alluvial fan gravel package). On the south-eastern (upthrown) side of the fault, this contact is well exposed in both walls of the trench. It is most uniform in the south-western wall, where it has an elevation on the trench log of -3.0 to -3.4 m (Figure 3.3). On the north-western side of the fault, the contact was exposed at an elevation of -8.2 m in a temporary pit excavated below the base of the trench. These values yield a vertical separation of between 4.8 and 5.2 m, with a median of 5.0 m.

The second feature is the difference in thickness of unit 4 (alluvial fan gravel package) either side of the fault: On the north-western (downthrown) side of the fault, the base of unit 4 has an elevation of -8.2 m, and the top has an elevation of -3.8 to -4.3 m, yielding a unit thickness of between 3.9 and 4.4 m. On the south-eastern side of the fault, the top of unit 4 has been partly deflated by colluvial activity, and its thickness somewhat reduced as a result. At the south-eastern end of the trench, farthest away from the zone of colluvial deflation, unit 4 is about 2.4

m thick. Therefore, unit 4 is between 1.5 and 2.0 m thicker on the downthrown side of the fault compared to the upthrown side.

The third feature is the contact between the top of unit 4 (alluvial fan gravel package) and the base of unit 3 (silt and gravelly silt package). The elevation of the top of unit 4 on the north-western side of the fault is -3.8 to -4.3 m, while the elevation of the top of this unit on the southeast side of the fault is -0.7 to -0.8 m, indicating a vertical separation of between 3.0 and 3.6 m, with a median of 3.3 m.

The fourth feature is the base of unit 3d across the fault zone (Figure 3.8A). At least 1 m of vertical buckling has deformed unit 3d, and this is regarded as a minimum estimate of vertical separation resulting from fault deformation.

Our approach for estimating the size of past single-event surface-rupture displacements on the Titri Fault at the Glenledi Road trench location is set out in the notes accompanying Table 3.1. In summary, we used the estimates of fault dip and amounts of vertical separation or unit thickness to calculate the total dip-slip displacement of each of the four geological features. We then divided those totals by our assessed minimum and likely maximum number of displacement events, to obtain a range of dip-slip single-event displacement values (SED). The difference in thickness of unit 4 gravel either side of the fault yields only a maximum estimate for SED, and we also note the question of whether the thickness difference is entirely due to faulting or may reflect natural irregularities due to stream channelling or erosion. The difference in height of unit 3d across the fault zone also yields only one estimate for SED, a minimum value that reflects the likelihood that the height difference only represents a part of the total deformation across the fault zone. The SED range obtained from the unit 4/unit 5 contact (top of bedrock) is 1.3 to 2.7 m, generated by a total of at least 3 surface ruptures, while the SED obtained from the top of unit 4 is between 1.0 and 2.8 m, produced by at least two surface ruptures. A strength of the estimates derived from these two geological features is that the features span the whole fault zone, thus capture all the deformation at the trench site, and across a time span of at least 2 rupture events. For our preferred working estimate of SED at this trench, we adopt the largest minimum value of 1.3 m, and smallest maximum value of 2.7 m, both derived from the unit 4/unit 5 contact. The median of that range is 2.0 m.

3.1.2 Assessment of timing of deformation events

A total of eight OSL samples were collected from trench T16/01 (Figures 3.3 and 3.4). Two samples, T16-01-OSL B and T16-01-OSL G (Figures 3.3 and 3.9), have been dated (Table 3.2). Both were analysed using the multiple aliquot additive dose (MAAD) method, and OSL B, from unit 4e, was also analysed using the single aliquot regenerative (SAR) method (Appendix 1).

Sample OSL B was collected from unit 4e near the top of unit group 4. The MAAD age of 50.0 ± 10.9 ka has a large uncertainty, but the SAR age of 36.5 ± 1.4 ka is much more precise and is regarded as a more representative maximum age for the occurrence of at least two, and possibly three or four, surface ruptures of the Titri Fault at this location. The 3 or 4 rupture possibility relates to option 1 described in the previous section, where unit 4 was deposited prior to the fault deformation recorded in the trench stratigraphy. Alternatively, by option 2 described in that section, at least one rupture occurred before the deposition of the upper part of unit 4. The earlier rupture(s) occurred before deposition of the strata dated by sample OSL B, and the latter two, or possibly three, ruptures occurred subsequently. We assign mutually equal weight to options 1 and 2.

Sample OSL G collected from the base of unit 2a, which was deposited after the most recent surface rupture event, returned an age of 11.4 ± 0.9 ka, and is a minimum age for the most recent surface rupture event at this location.

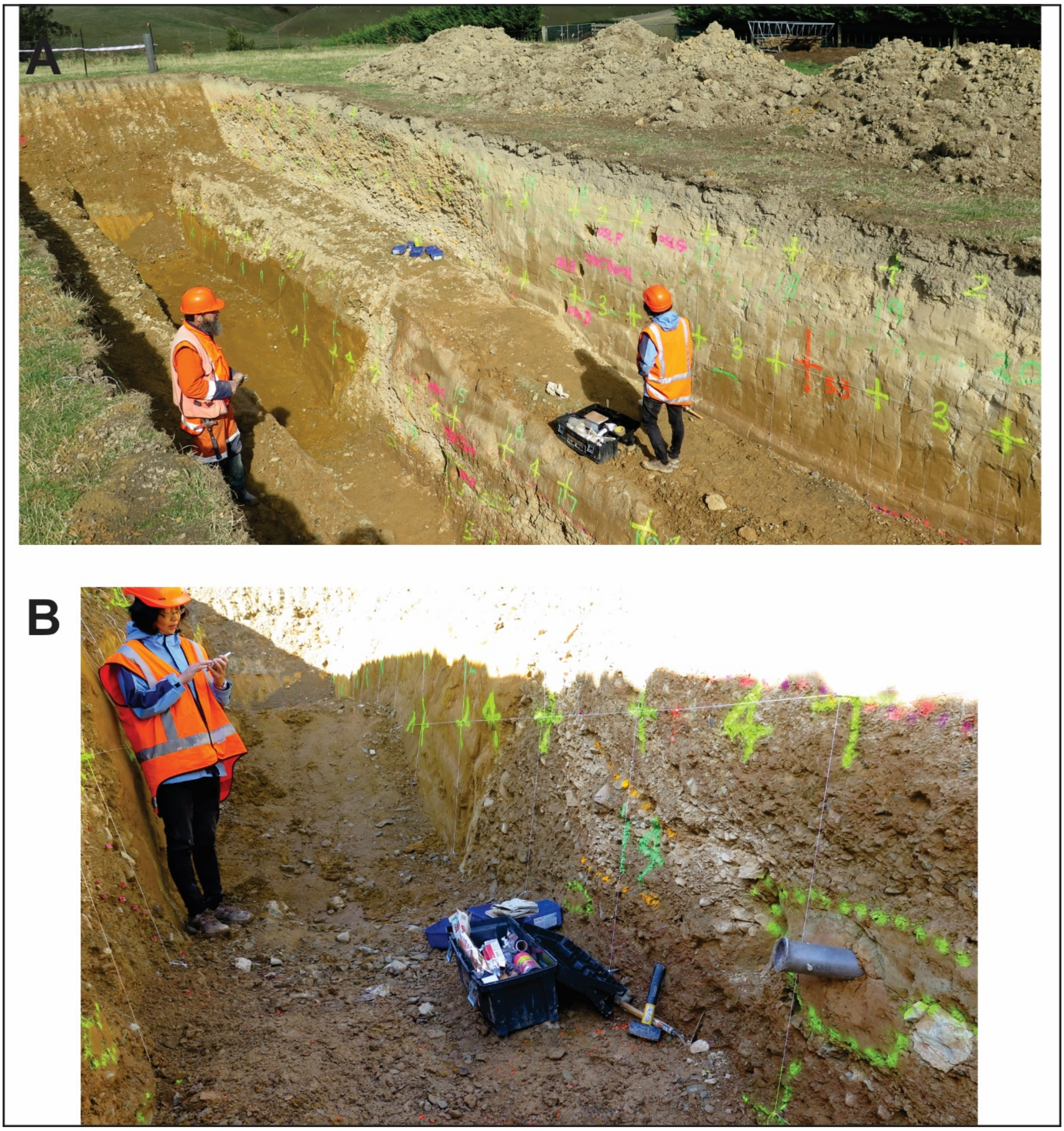

Figure 3.9 Samples for dating from Glenledi Road trench T16/01. A: Geologist Van Dissen and geochronologist Wang reflect upon the successful collection of six samples for OSL dating (holes marked by pink paint) from the south-western wall of the trench. Photo: GNS Science, D.J.A. Barrell. B: The steel driving tube (lower right) has been hammered into a silt pod (unit 4e within unit 4d alluvial fan gravel), and the stainless-steel tube containing sample T16/01-OSL B lies inside the silt pod, awaiting extraction. Those strata have experienced at least two, and possibly three, fault ruptures. The laboratory-measured age of the OSL B sample (36.5 ± 1.4 ka - Figure 3.3) is a maximum age for those rupture events. Photo: GNS Science, D.J.A Barrell.

Table 3.2 Dating results for the Titri Fault trenches. Sample locations, along with dating results, are shown on the trench logs. Type column identifies the dating method used; Optically stimulated luminescence (OSL) or radiocarbon (^{14}C). In tectonic context, MRE is the most recent surface-rupture event and PE is the penultimate surface-rupture event. OSL ages are by the multiple aliquot additive dose method (MAAD), unless identified as the single aliquot regenerative method (SAR).

Sample Name (Lab number)	Type	Description/Depth Below Ground Level (bgl)	Tectonic Context of Sample	Age
Glenledi Road trench				
Titri T16-01 - OSL B (WLL1211)	OSL	Bed of silty sand (unit 4e) in stream gravel (unit 4d)/3.35 m bgl	Older than at least two surface ruptures	50.0 ± 10.9 ka and 36.5 ± 1.4 ka (by SAR)
Titri T16-01 - OSL G (WLL1212)	OSL	Silt-clay (unit 2b)/0.75 m bgl	Definitely younger than MRE	11.4 ± 0.9
Clarendon trenches				
Titri T16-02 - OSL A (WLL1213)	OSL	Silty sand (unit 'A') under organic beds (units 'B', 'C')/ 2.95 m bgl	Inferred to be older than at least two surface ruptures	75.3 ± 9.5 ka and 70.6 ± 3.5 ka (by SAR)
Titri T16-02 - 14C B (NZA 62203)	^{14}C	Thin organic layers within unit 'C'/ 2.7 m bgl	Inferred to be older than at least two surface ruptures	Background (older than ~50 ka)
Titri T16-02 - OSL E (WLL1214)	OSL	Silt (unit 'F3') within upper grit-free silt-clay/0.70 m bgl	Definitely younger than MRE	20.0 ± 1.7 ka
Titri T16-03 - OSL A (WLL1215)	OSL	Bed of silty sand (unit 4a) in stream gravel (unit 4b)/1.50 m bgl	Older than at least two surface ruptures	42.0 ± 4.3 ka
Titri T16-03 - OSL D (WLL1216)	OSL	Slightly gravelly silt-clay (unit 3c)/2.00 m bgl	Definitely younger than PE; definitely older than MRE	29.4 ± 1.9 ka
Titri T16-03 - OSL G (WLL1217)	OSL	Silt-clay (unit 2a), below stone line/0.95 m bgl	Definitely younger than MRE	16.7 ± 1.1 ka and 16.7 ± 0.4 ka (by SAR)

3.2 Clarendon (trenches T16/02 and T16/03)

The Clarendon trenching locality lies about 7 km northeast of the Glenledi Road trench site, about 10 km northeast of Milton and 40 km southwest of Dunedin (Figure 1.1). A detailed location map is provided in Figure 3.10. The locality is on a small alluvial fan deposited by an unnamed stream draining northwest from a small catchment (~1 km^2) in eroded hill terrain. The geology of the catchment comprises Otago Schist overlain by Henley Breccia, according to the geological map of Bishop (1994).

3.2.1 Excavation sequence

The target feature was a northeast-trending step, up to the southeast, across a northwest-draining alluvial fan (Figures 3.10 and 3.11). The step’s orientation, and position at the north-western margin of rolling hill country, led us to interpret it as a possible fault scarp. Trench T16/02 was sited at the lowest, north-eastern, end of the suspected scarp, in anticipation of exposing un-faulted sediments overlying faulted sediments, thus providing preand post-faulting dating targets. However, we found blue-grey clays whose poorly-drained character suggested that they lay on the downthrown side of the fault. We halted excavation and instead dug across the prominent scarp to establish whether or not a fault was present. The new trench T16/03 confirmed faulting. The digger was relocated to T16/02 and lengthened it to the southeast (collectively, trench footprint in Figure 3.10). The reason for lengthening was that the geological deposits in T16/02 (Figure 3.12) appeared to be un-faulted and dating of them would place useful limits on when the most recent Titri Fault surface rupture occurred here. It was therefore important, if possible, to confirm them as being un-faulted.

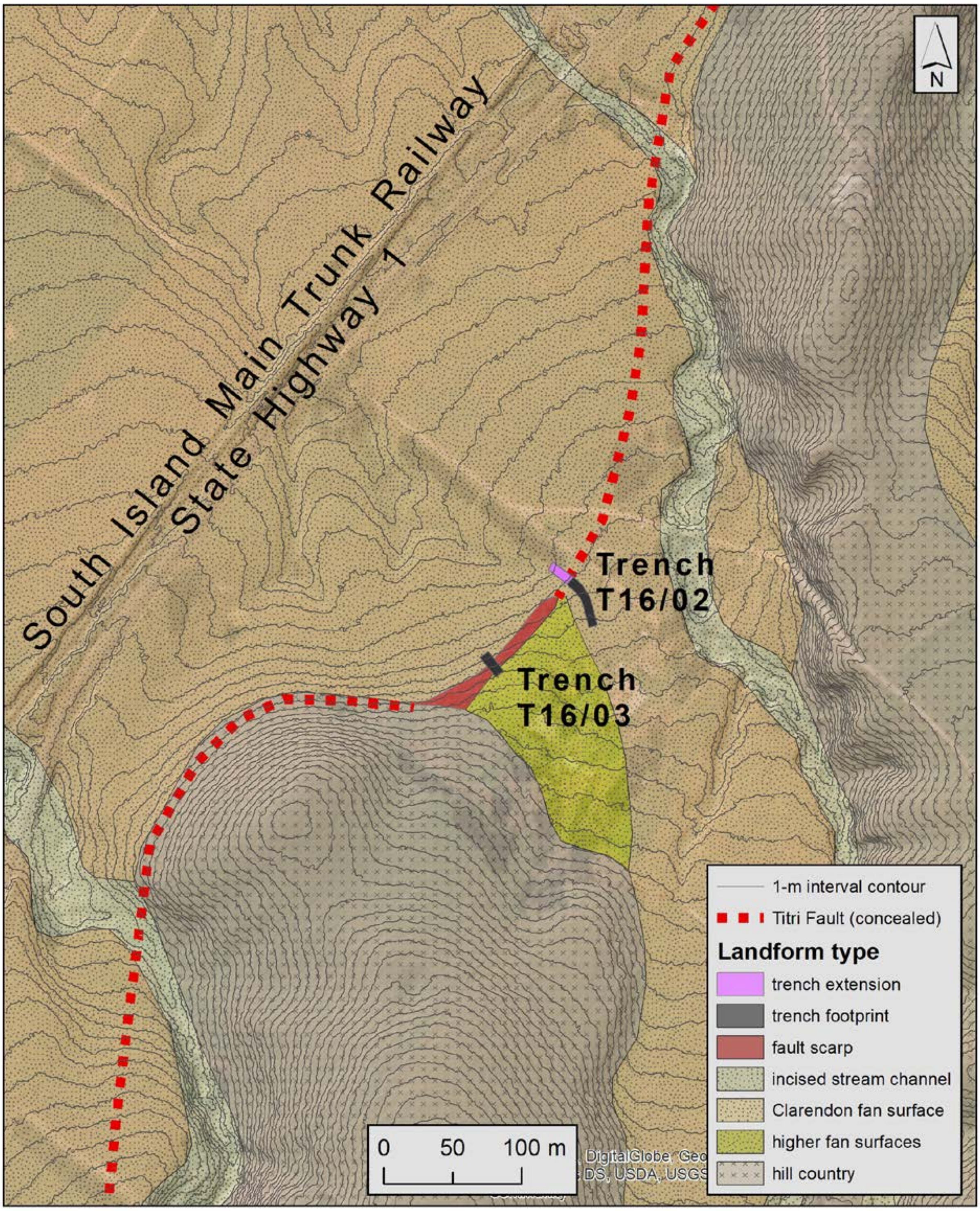

Figure 3.10 Location map and landform interpretation for the Clarendon trench sites. Background of figure is a transparent aerial photo draped on the lidar hill shade model.

Following the logging and peer review of trench T16/03, and especially the measurement of fault orientations in the trench, we concluded that despite the nature of sediments exposed in T16/02, the fault was more likely to project to the northwest of T16/02. Therefore, when the trenches were being backfilled, T16/02 was extended about 10 m to the northwest, and successfully intersected fault-deformed alluvial sediments (trench extension, Figure 3.10). This showed that many of the older units exposed in the original trench that we had thought to be un-faulted were in fact faulted. We present the Clarendon trench results in the order that best elucidates and constrains the style, timing and amount of faulting events at this site, first by addressing trench T16/03 (Figure 3.13) and then trench T16/02.

Figure 3.11 Views of the Clarendon trenching locality. A: Looking northeast along the morphologically subdued fault scarp. Beyond the white vehicle is the T16/02 spoil pile and the excavation of T16/03 is in progress. Photo: GNS Science, D.J.A. Barrell. B: Looking southeast towards the fault scarp, where trench T16/03 is being excavated. Photo: GNS Science, D.J.A Barrell.

Figure 3.12 Views of trench T16/02 in early April 2016, prior to its extension in late April 2016. A: The team is marking out stringlines and meterages in this view southeast up the trench. In the distance, the change in trench trend was done to follow the fall-line of the alluvial fan surface. Photo: GNS Science, D.J.A. Barrell. B: Geologists Hornblow (in chair), Litchfield (standing) and Van Dissen (sitting) are logging the north-eastern wall of the trench. The distinctive blue-grey clay near the trench floor is ponding groundwater seepage from up-trench. Subsequent extension of the trench to the northwest uncovered the fault, approximately under the spot where geologist Litchfield is standing. Photo: GNS Science, D.J.A Barrell.

3.2.2 Trench T16/03

Trench T16/03 exposed alluvial fan gravels with thin layers of sand or silt (unit group 4) overlain by gravelly sands and silts (unit groups 3 and 2) (Figures 3.13, 3.14, and 3.15). Both unit groups 4 and 3 are deformed by the fault but unit group 2 is not, indicating that those sediments were deposited after the most recent fault deformation at this location. Fault displacement information from the trench is collated in Table 3.3.

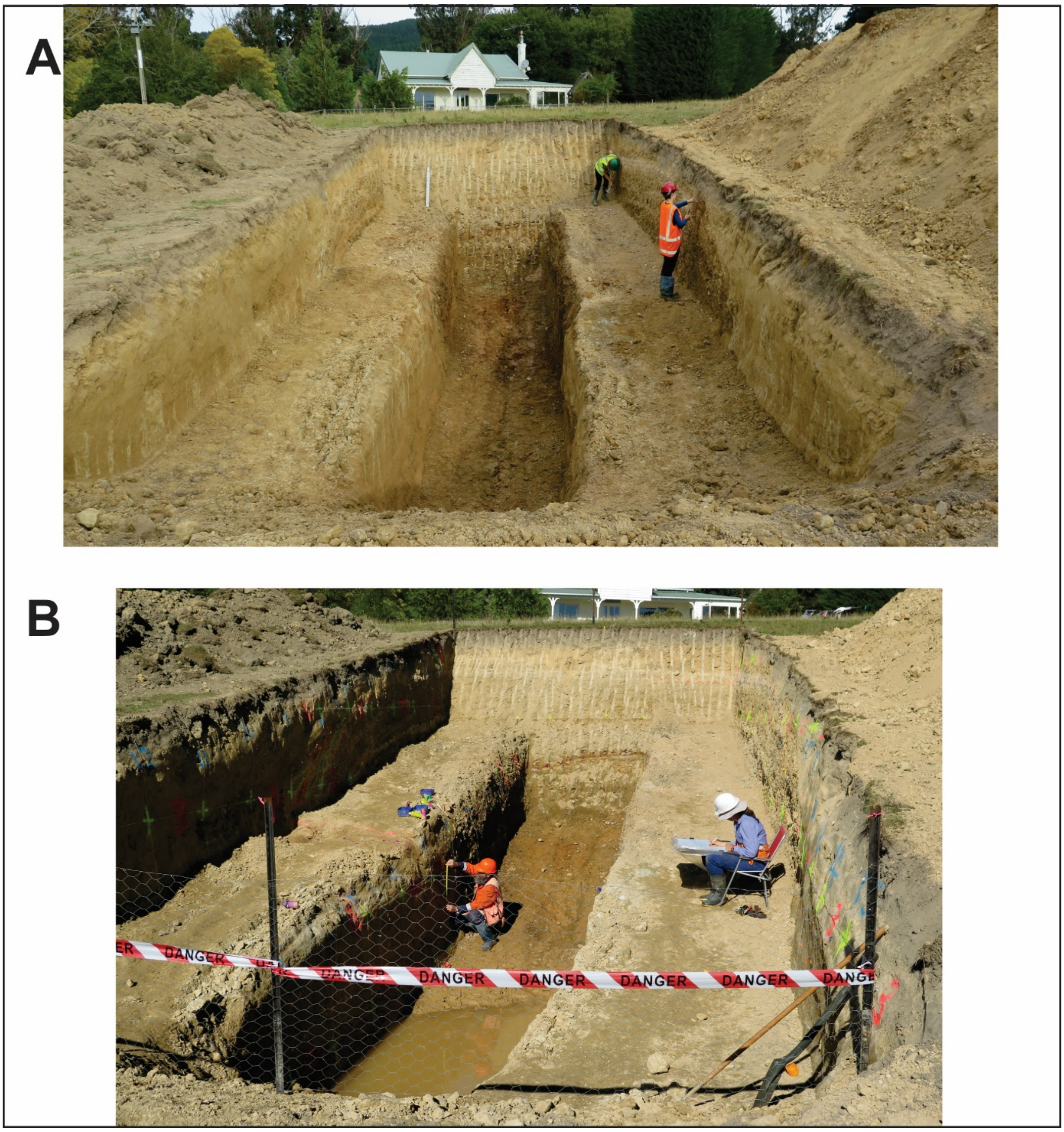

Figure 3.13 Views of trench T16/03 during gridding and logging. A: Geologists Taylor-Silva and Hornblow stringing out the grid on the south-western wall. Photo: GNS Science, D.J.A. Barrell. B: Geologists Van Dissen and Litchfield logging the north-eastern wall. Photo: GNS Science, D.J.A Barrell.

3.2.2.1 Assessment of fault deformation

Trench T16/03 exposed a well-resolved zone of fault offset and buckling of alluvial fan sediments (Figures 3.14, 3.15, and 3.16). In the south-western wall, the fault planes are clearly expressed with two faults that merge upwards and dip gently to the southeast (24° and 34°, Figure 3.14). In the north-eastern wall, the fault zone comprises three subparallel faults and is somewhat steeper (47° dip southeast; Figure 3.15). All of the faults show a reverse sense of throw and unit 4 on either side is buckled, with the amount of buckling increasing towards the fault. There are also several fissures (subvertical cracks cutting through units 4a-4c) on the upthrown side, which likely formed as a result of the buckling.

The south-western wall shows perhaps the clearest evidence in any of the trenches for at least two faulting events. The oldest event displaced unit group 4 and formed a fault scarp. Erosion of the scarp is interpreted to have formed gravelly silt unit 3c, which is thought to be a wedge of material shed off the newly-formed fault scarp. Alluvial fan gravel of unit 4b has then been displaced up and over units 3b and 3c in a subsequent fault rupture event (Figure 3.17A). Unit 2b is interpreted to be a colluvial wedge that formed after this event. Units 2a and 2b are un-faulted, and therefore are younger than the most recent surface rupture at this location.

A feature of this trench is the presence of several fissures on the upthrown side of the fault (Figure 3.16). Their position within a zone of bending close to the fault suggests that they most likely formed co-seismically in association with buckling of the strata. The presence of silty gravel (unit 3a) extending down into some of the fissures provided a rationale for differentiating unit 3a – which presumably was in place prior to the most recent movement, or perhaps an earlier movement, during which the fissures were formed – from the unit 2a colluvium that everywhere in this trench appears to be un-faulted (Figures 3.14 and Figure 3.15). In the north-eastern wall, one of the fissures has silt of unit 4c extending up into the fissure, suggesting that some upward injection of 4c silt occurred at the time the fissure was formed.

Two geological features are considered sufficiently distinctive across the fault zone to provide useful estimates of amounts of fault displacements. They are listed in Table 3.3 and described below.

Contact between top of unit 4 and base of unit 3 (SW wall): The elevation of the top of unit 4 on the southeast side (upthrown side) of the fault is -1.0 to -1.1 m on the trench log, while the elevation of the top of this unit on the northwest side of the fault is -4.4 to -4.6 m, indicating a vertical separation of 3.3 to 3.6 m. There is the possibility that some erosion has taken place across the top of unit 4 in the hanging-wall, so we regard this vertical separation as a minimum value. Measurement of the offset of this contact along the fault plane results in a minimum dip-slip displacement of 2.2 m, which does not take account of hanging-wall folding.

Contact between top of unit 4 and base of unit 3 (NE wall): The elevation of the top of unit 4 on the southeast side (upthrown side) of the fault is -1.1 m at the south-eastern end of the trench, while the elevation of the top of this unit on the northwest side of the fault is -4.7 m at the north-western end of the trench, indicating a vertical separation of 3.6 m. There has been erosion of this unit on the hanging-wall side of the fault, so we regard this vertical separation as a minimum value. Measurement of the offset of this contact along the fault plane results in a minimum dip-slip displacement of 1.1 m, which does not account for hanging-wall folding.

Thickness of unit 2b proximal of the fault (SW & NE walls): unit 2b is interpreted to be a colluvial wedge formed as a result of the most recent surface fault rupture. The thickness of unit 2b proximal to the fault (0.7–0.8 m) is regarded as a minimum estimate of the vertical displacement that occurred in the most recent rupture. Taking the maximum fault dip of 47°, we convert the minimum vertical displacement to a minimum dip-slip displacement of 1.0 and 1.1 m in the SW and NE walls, respectively.

Following the same process used for the Glenledi Road trench, namely dividing the dip-slip displacements by the number of events, we calculate minimum single event displacements (SED) ranging from 0.6 to 2.5 m (Table 3.3). Of these values, the unit 4/3 contact is considered the best available marker for measuring single event displacement because it captures at least two events and the majority of the deformation due to those events, so we take the average value of 2.4 m as the best minimum SED at the Clarendon T16/03 trench site.

This page left intentionally blank.

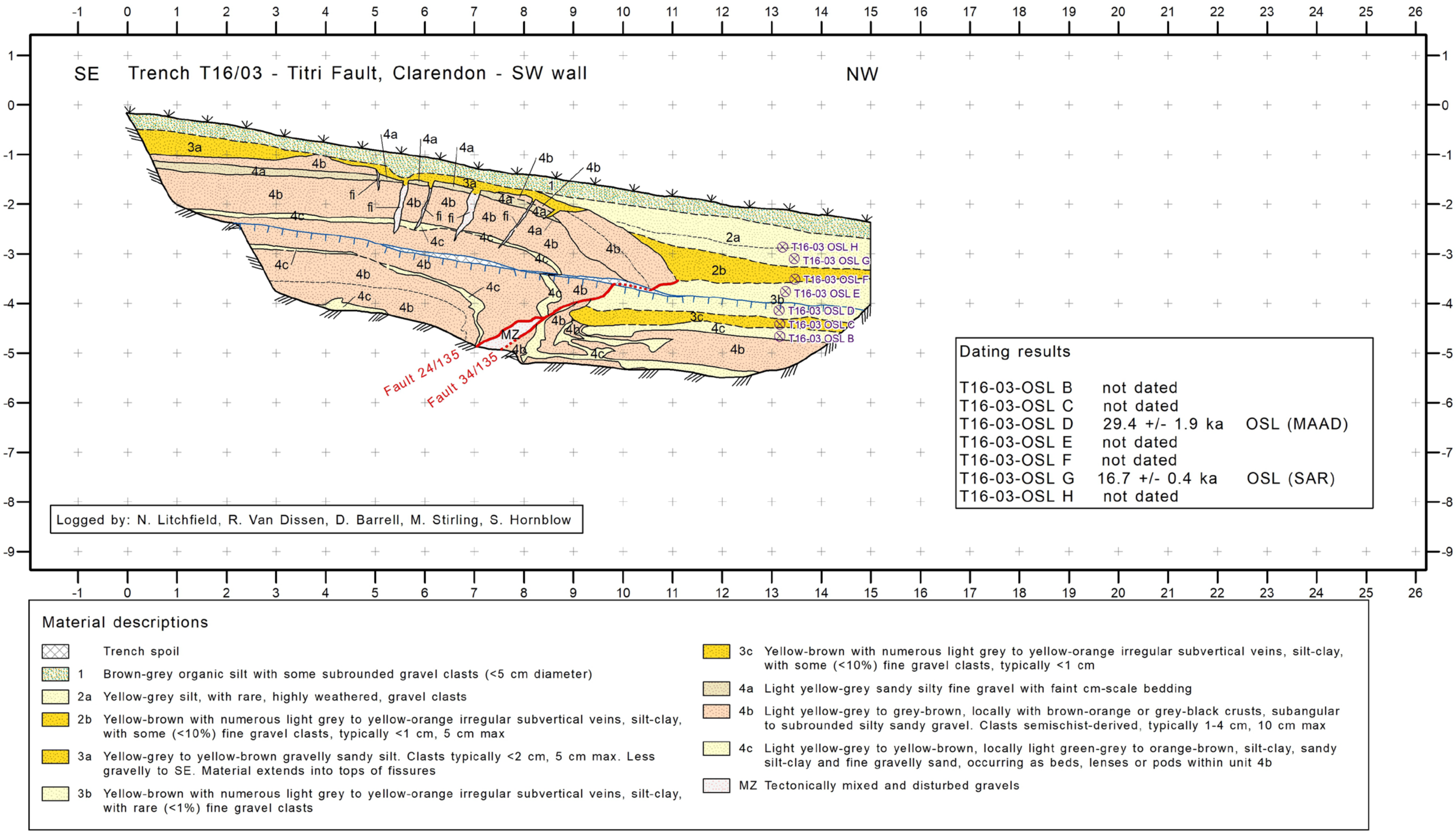

Figure 3.14 Log of Trench T16/03, south-western wall. Log axes are in metres. The fault attitudes are field measurements and an overall dip estimate for the fault is given in Table 3.3. Unit 'fi' is MZ material within fissures. Minor discontinuous units within a more extensive unit are labelled in smaller font. More information on the dating samples and results is presented in Table 3.2.

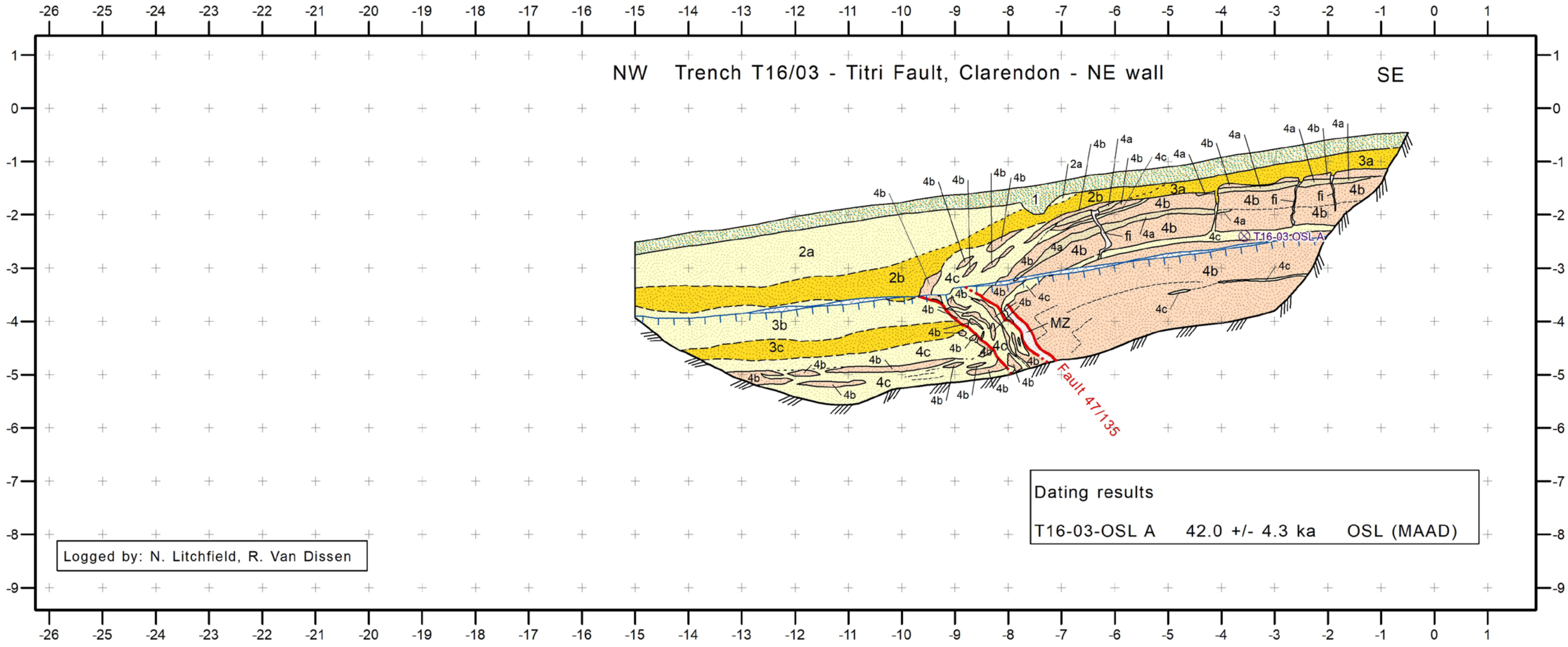

Material descriptions

	Trench spoil
1	Brown-grey organic silt with some subrounded gravel clasts (<5 cm diameter)
2a	Yellow-grey silt, with rare, highly weathered, gravel clasts
2b	Yellow-brown with numerous light grey to yellow-orange irregular subvertical veins, silt-clay, with some (<10%) fine gravel clasts, typically <1 cm, 5 cm max
3a	Yellow-grey to yellow-brown gravelly sandy silt. Clasts typically <2 cm, 5 cm max. Less gravelly to SE. Material extends into tops of fissures
3b	Yellow-brown with numerous light grey to yellow-orange irregular subvertical veins, silt-clay, with rare (<1%) fine gravel clasts
3c	Yellow-brown with numerous light grey to yellow-orange irregular subvertical veins, silt-clay, with some (<10%) fine gravel clasts, typically <1 cm
4a	Light yellow-grey sandy silty fine gravel with faint cm-scale bedding
4b	Light yellow-grey to grey-brown, locally with brown-orange or grey-black crusts, subangular to subrounded silty sandy gravel. Clasts semischist-derived, typically 1-4 cm, 10 cm max
4c	Light yellow-grey to yellow-brown, locally light green-grey to orange-brown, silt-clay, sandy silt-clay and fine gravelly sand, occurring as beds, lenses or pods within unit 4b
MZ	Tectonically mixed and disturbed gravels

Figure 3.15 Log of Trench T16/03, north-eastern wall. Log axes are in metres. The fault attitude is a field measurement and accords with the overall fault-dip estimate given in Table 3.3. Unit 'fi' is MZ material within fissures. Minor discontinuous units within a more extensive unit are labelled in smaller font. More information on the dating samples and results is presented in Table 3.2.

Table 3.3 Clarendon trench T16/03 fault displacement information. The values have been estimated from the trench logs (Figure 3.14 and Figure 3.15. Fault dip values differ from fault attitudes on the logs that were measured in the field on localised sectors of the fault planes.

Geological Feature	Fault Dip (degrees)			Vertical Separation (m)			Dip-slip Displacement (m)			Estimated Number of Surface-Rupture Events	Average Dip-Slip Single-Event Displacement (m)	
	average	minimum	maximum	median	minimum	maximum	average	minimum	maximum		minimum	maximum
Contact between top of unit 4 and base of unit 3 (SW wall)	41°	34°	47°	-	3.3	-	-	4.5	-	2	2.3	-
Contact between top of unit 4 and base of unit 3 (NE wall)				-	3.6	-	-	4.9	-	2	2.5	-
Contact between top of unit 4 and base of unit 3 as measured along the fault plane (SW wall)	-	-	-	-	-	-	-	2.2	-	2	1.1	-
Contact between top of unit 4 and base of unit 3 as measured along the fault plane (NE wall)	-	-	-	-	-	-	-	1.1	-	2	0.6	-
Thickness of unit 2b above the fault tip (SW wall)	41°	34°	47°	-	0.7	-	-	1.0	-	1	1.0	-
Thickness of unit 2b above the fault tip (NE wall)				-	0.8	-	-	1.1	-	1	1.1	-

NOTES

Fault dip values were estimated from the logs using a protractor. The fault zone exposed in the south-western wall of the trench has an overall dip of 34°, while in the north-eastern wall the overall dip is 47°. These are taken as representative minimum and maximum dips, and together give an average dip of 41°. These fault dip values are applied to each of the geological features listed in the table.

Vertical separation of each geological feature across the fault zone is taken from the logs.

Vertical separation of each geological feature across the fault zone is taken from the logs, and includes representative estimates of maximum and minimum separation, based on plausible options for projection of each geological feature into the fault zone (see text for additional information). The median value is midway between the minimum and maximum.

Dip-slip displacement is calculated from the fault dip and vertical separation. The minimum value comes from maximum fault dip and minimum vertical separation.

The estimated numbers of single-event displacement events refer to the number that produced the vertical separation of each geological feature and are discussed further in the text.

The dip-slip single-event displacement is the dip-slip displacement value divided by the number of single-event displacements. The minimum value is based on the minimum displacement and larger estimate of events, while the maximum value comes from the maximum displacement and smaller estimate of events.

This page left intentionally blank.

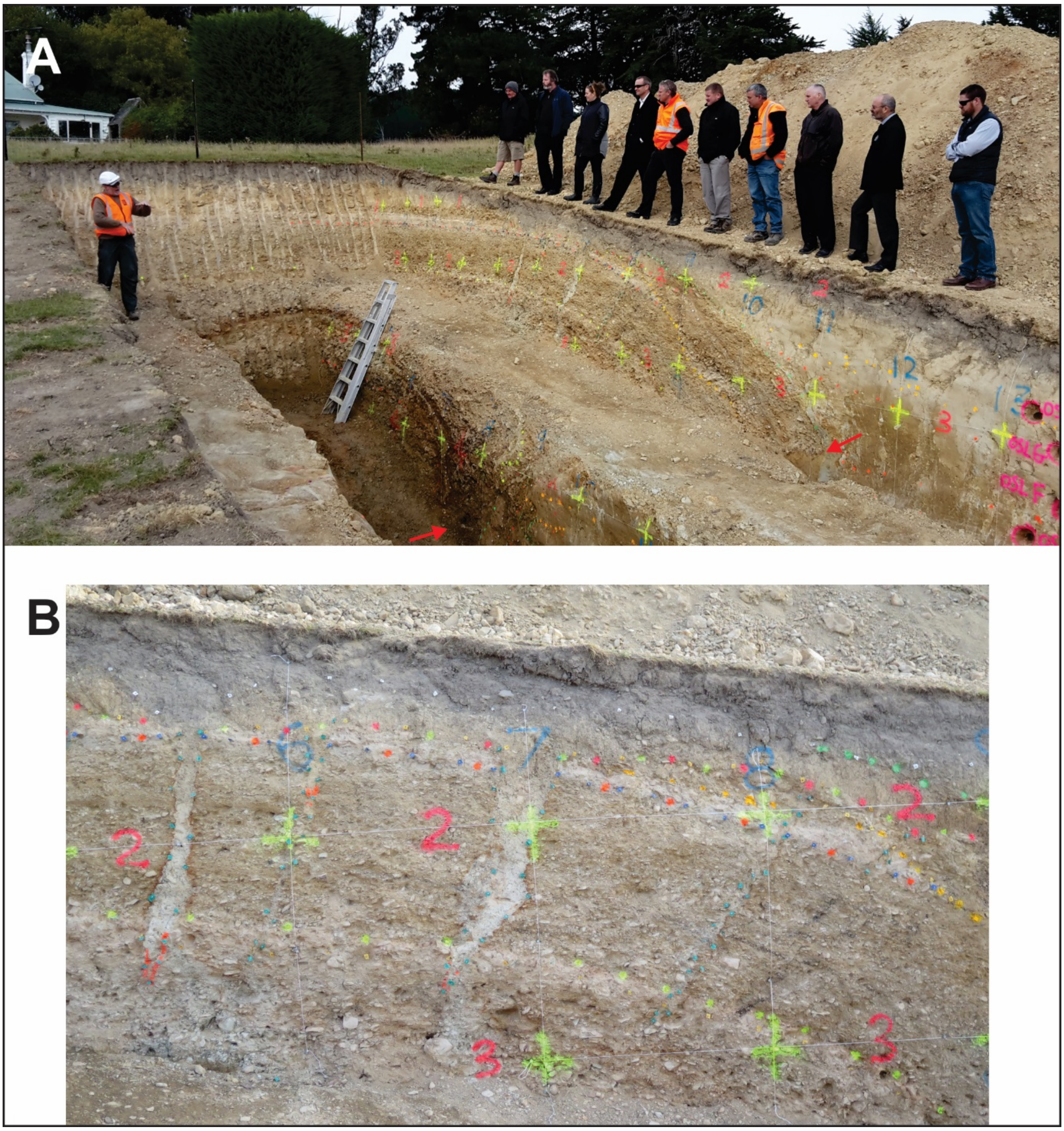

Figure 3.16 Views of fault-deformation features in trench T16/03. A: Geologist Barrell explains the features exposed in the trench to a visiting group of staff from local authorities through whose areas the Titri Fault passes (Clutha District Council, Dunedin City Council and Otago Regional Council). Note the bending of gravel layers on the upthrown side of the fault, the location of which is marked by red arrows. Light-coloured infilled fissures associated with the bending, visible below the four bystanders on the left, are detailed in photo B. Photo: GNS Science, R. Smillie. B: Detail of infilled fissures within unit 4 alluvial fan sediments in the south-western wall of the trench, between meterages 5 and 9 horizontal and -1.5 and -3 vertical (Figure 3.14). In places, the overlying yellow-brown gravelly silt colluvium (unit 3a) extends down into the fissures, adjoining the mixture of fissure-wall sediments and silt that forms most of the fissure-fill (unit MZ). Photo: GNS Science, D.J.A Barrell.

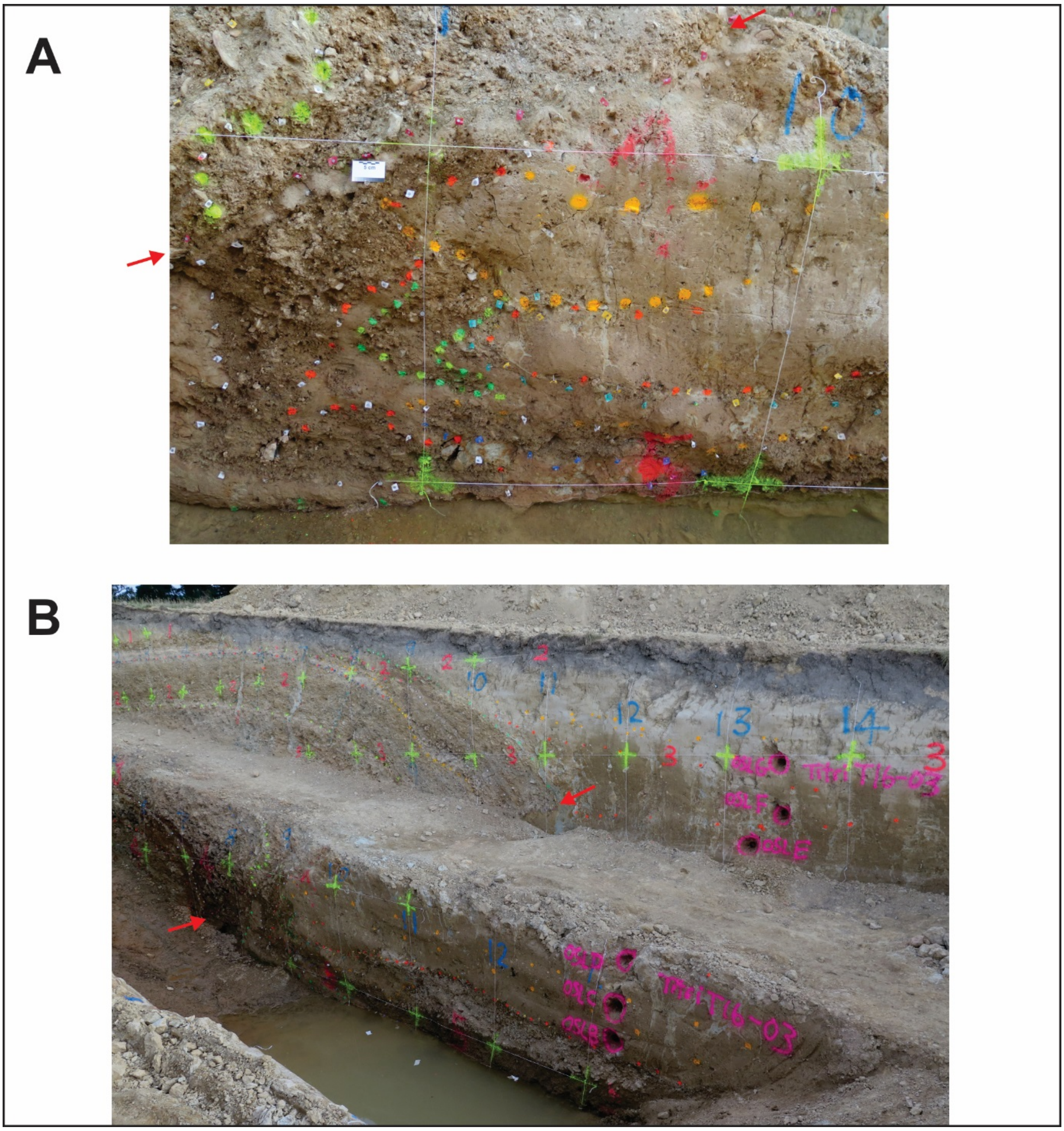

Figure 3.17 Views of trench T16/03, showing fault-deformation features and sample locations. A: In the south-western wall, at meterages 8.5 to 10 horizontal and -4.5 to -5 vertical (Figure 3.14), nearly horizontal colluvial unit 3c (orange dots) overlies highly buckled unit 4 alluvial fan sediments (red and green-blue dots). At upper left, unit 4 gravelly sediments were subsequently thrust over unit 3 silty sediments. Photo: GNS Science, D.J.A. Barrell. B: The south-western wall of the trench exposes warped gravel-dominated sediments (unit 4) faulted up (red arrows) and over silt-dominated unit 3 sediments. Two of the six OSL samples (holes marked by pink paint) have been dated (OSL D just below the bench, and OSL G in the upper batter. Photo: GNS Science, D.J.A Barrell.

3.2.2.2 Assessment of timing of deformation events

Three OSL ages were obtained from this trench (Figure 3.14, Figure 3.15, and Table 3.2). Sample T16-03-OSL A was collected from unit 4c in the north-eastern wall and returned an age of 42.0 ± 4.3 ka (Figure 3.15). As previously discussed, unit 4c is interpreted to have experienced at least two surface rupture events, based on stratigraphic and fault relationships. Accordingly, the older age bound of OSL A (i.e. 46.3 ka) provides a maximum age for at least two surface rupture events.

In the south-western wall (Figure 3.14), a sample from unit 3b, thought to have been deposited during the time interval between two surface rupture events, yielded an age of 29.4 ± 1.4 ka (T16-03-OSL D). The younger bound of that age (i.e. 27.5 ka) is a minimum age for a previous fault rupture event, while the older bound (i.e. 31.3 ka) is a maximum for the most recent surface fault rupture event at this location.

The third sample dated from this trench, T16-03-OSL G, was collected from the base of un-faulted unit 2a and yielded a SAR age of 16.7 ± 0.4 ka, the younger bound of which (i.e. 16.3 ka) is a minimum age for the most recent surface rupture event at this location.

3.2.3 Trench T16/02

Trench T16/02 exposed a series of nearly horizontal sands and clays (unit group 4) locally overlying bedrock (unit 5) near the fault (Figures 3.18, 3.19, 3.20, 3.21, and 3.22). The bedrock is characterised by the presence of pure quartz gravel lenses (unit 5b), which contrast profoundly with the semi-schist gravel that dominates the alluvial fan sediments. The bedrock is considered likely to be Wangaloa Formation (~66–34 Ma) and the contact between units 5 and 4 is likely to have been eroded by stream action. Unit 4 is overlain by gravelly sands and silts (unit groups 3 and 2) and the deposition of unit group 2 is interpreted to have occurred after the most recent fault deformation at this location. Fault displacement information from the trench exposure is collated in Table 3.4.

A feature of this trench is the presence of some organic remains in the sediments, considered potentially suitable for radiocarbon dating. Unit 4b contains some dark organic layers and unit 4d comprises blue-grey clay with many dark flecks of organic matter (Figure 3.23). Likely to have been formed in a stream-margin swamp environment associated with the alluvial fan at this location, unit 4d was particularly valuable because it is an unusual and distinctive sediment and could readily be identified on both sides of the fault. It is well exposed on the upthrown side (Figure 3.12B, 3.23) and was successfully encountered in the temporary test pit on the downthrown side Figure 3.18.

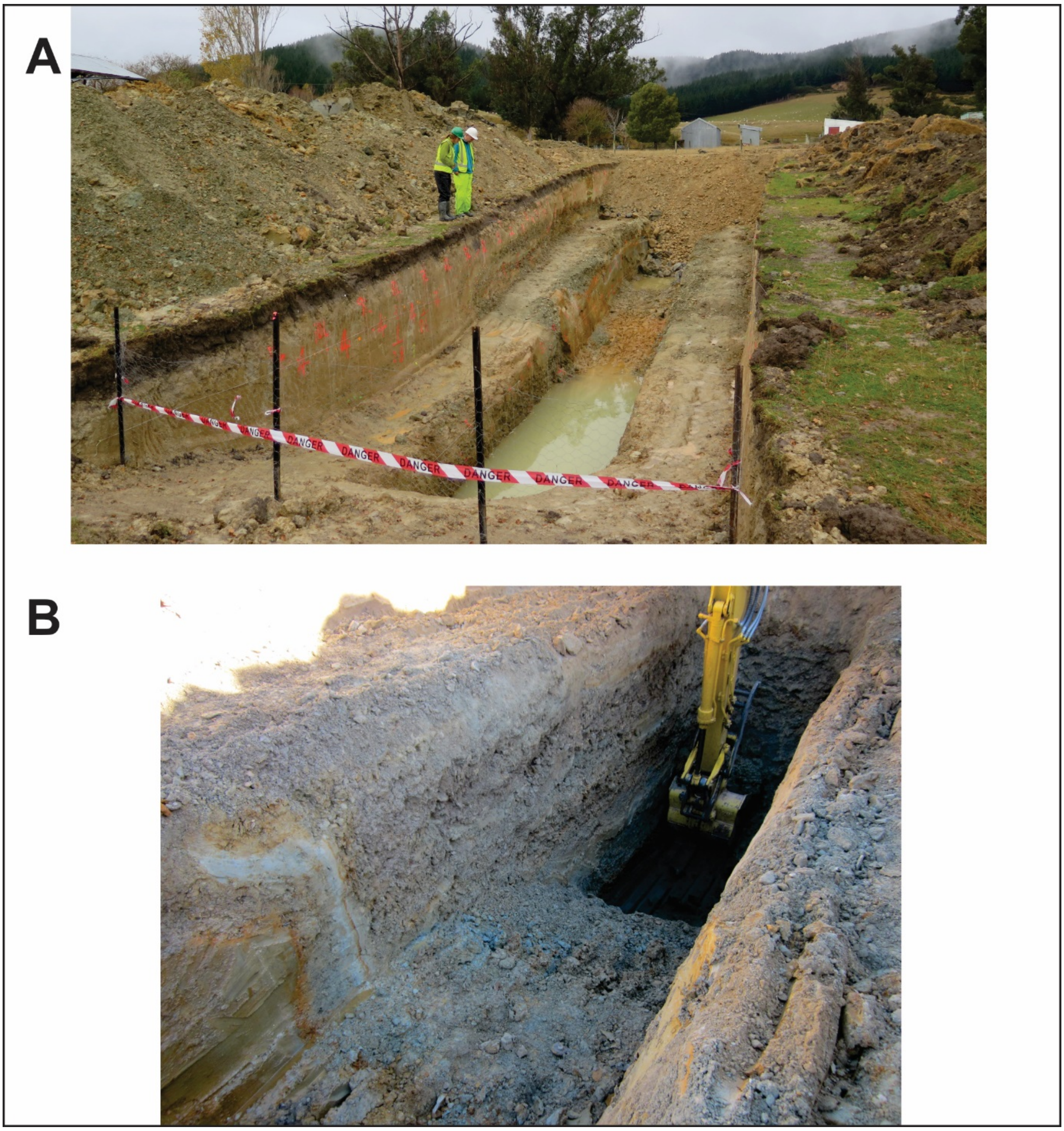

Figure 3.18 Views of the extension of trench T16/02. A: Geologists Taylor-Silva and Stirling stand above the exposure of the Titri Fault in the trench. In this view to the southeast, alluvial fan gravel has been faulted up against silt-dominated deposits in the foreground. The south-eastern part of the trench has already been backfilled. Photo: GNS Science, D.J.A. Barrell. B: The digger is excavating a temporary test pit at the northwest end of the trench extension. It has just unearthed the dark-coloured clay of unit 4d beneath grey-brown alluvial fan gravel of units 3d/4a (Figure 3.20 and Figure 3.22). This provides a critical geological element for determining the amounts of offset across the fault. Photo: GNS Science, D.J.A Barrell.

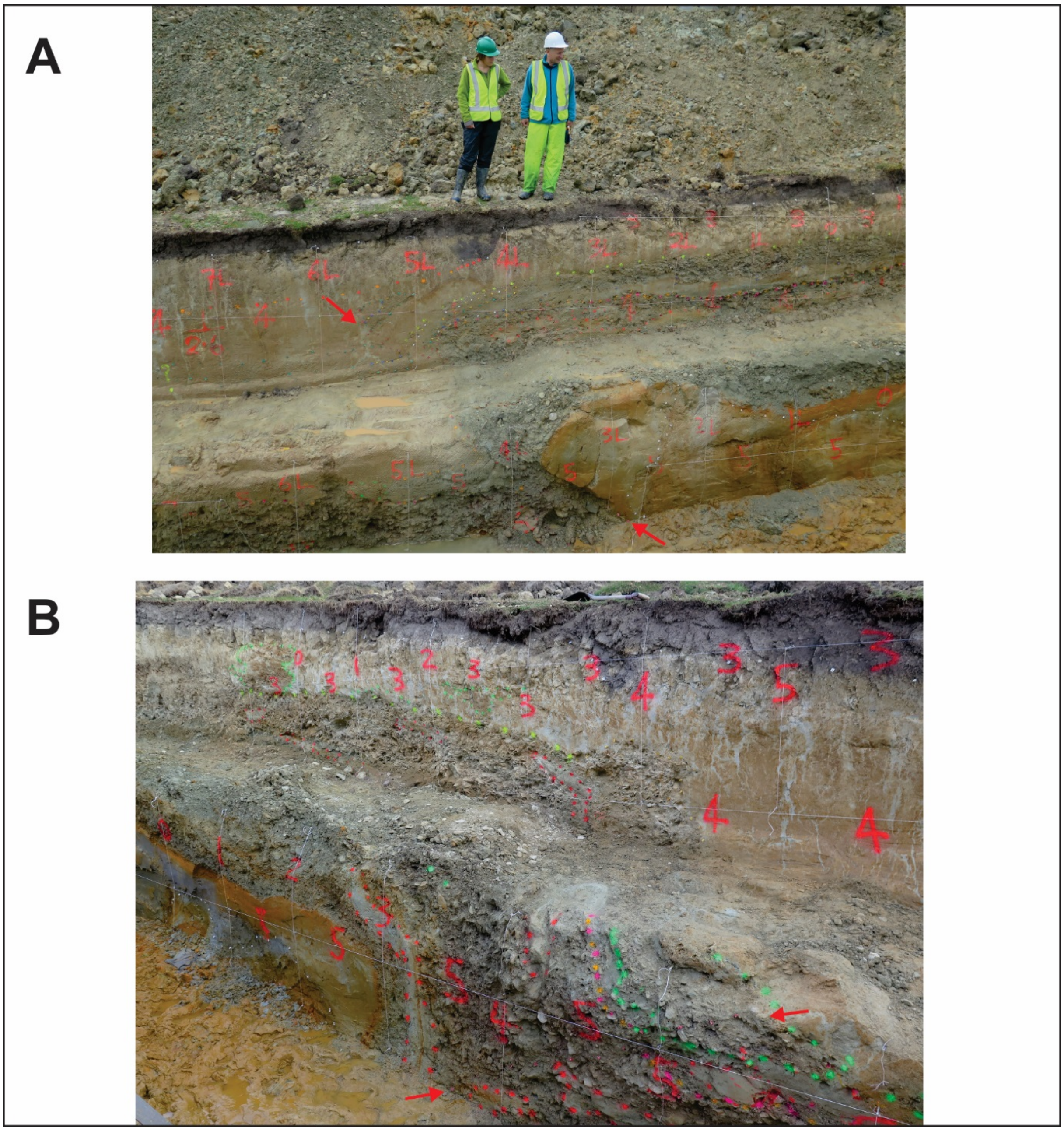

Figure 3.19 Views of the fault deformation in trench T16/02. A: Geologists Taylor-Silva and Stirling stand above the well-defined fault offset (red arrows) in the north-eastern wall of the trench. Photo: GNS Science, D.J.A. Barrell. B: Looking south towards the south-western wall, the deformation consists mainly of buckling of the strata, with only a small discrete fault offset (red arrows) recognisable. Photo: GNS Science, D.J.A Barrell.

This page left intentionally blank.

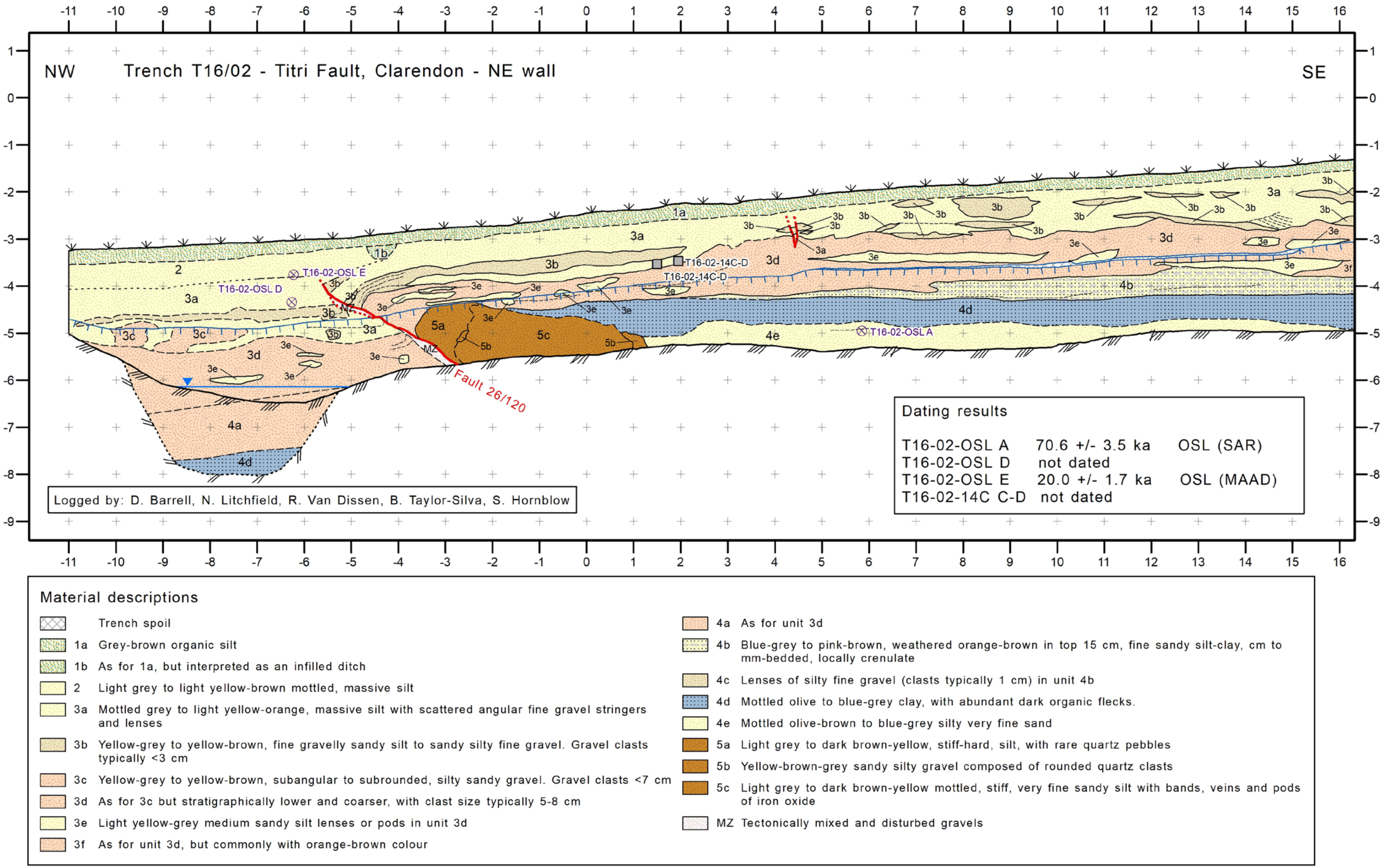

Figure 3.20 Log of Trench T16/02, north-eastern wall, sheet 1. Log axes are in metres. The fault attitude is a field measurement and differs from the representative fault-dip values given in Table 3.4 and discussed in the text. Minor discontinuous units within a more extensive unit are labelled in smaller font. More information on the dating samples and results is presented in Table 3.2.

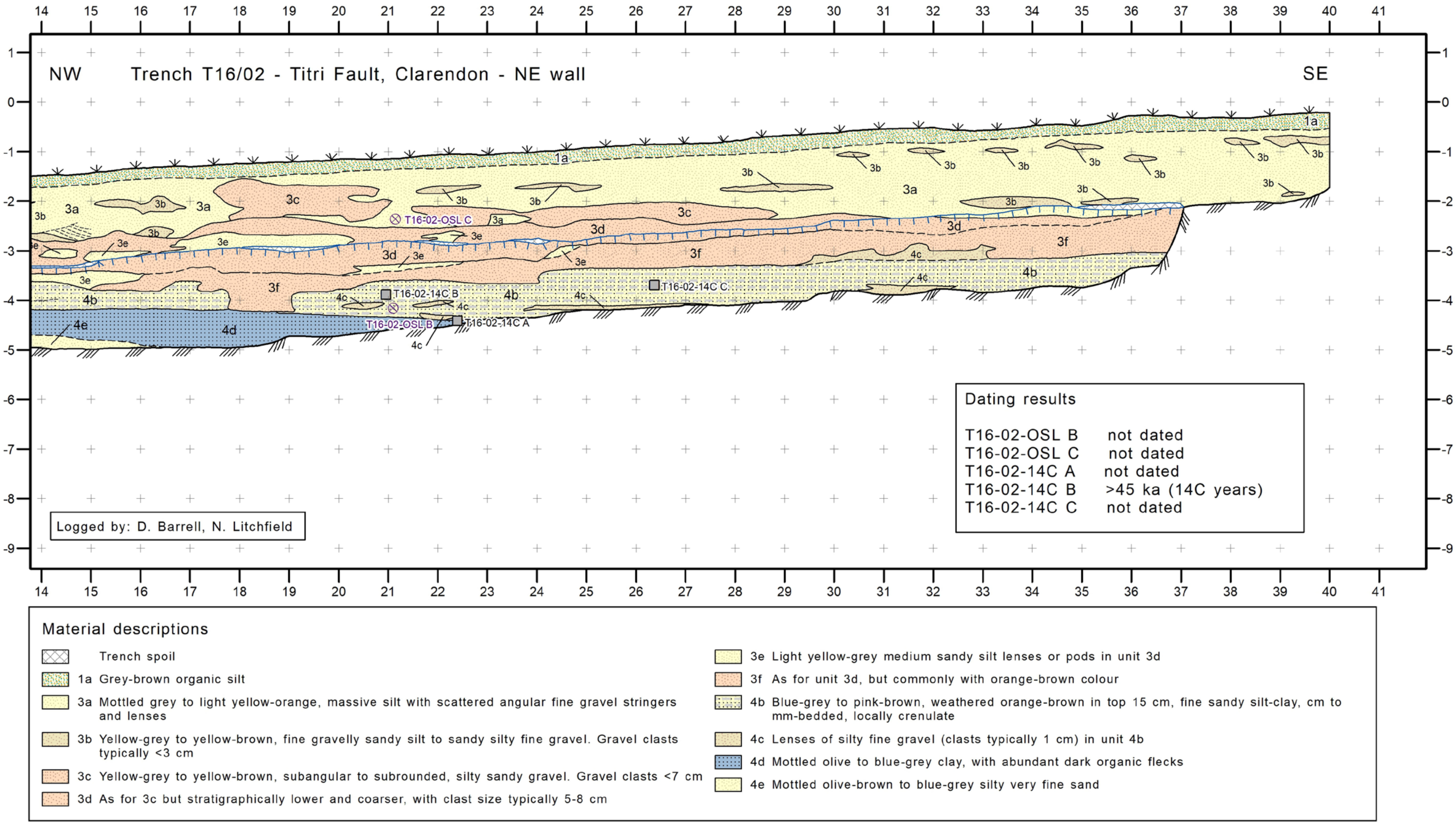

Figure 3.21 Log of Trench T16/02, north-eastern wall, sheet 2. Log axes are in metres. Minor discontinuous units within a more extensive unit are labelled in smaller font. More information on the dating samples and results is presented in Table 3.2.

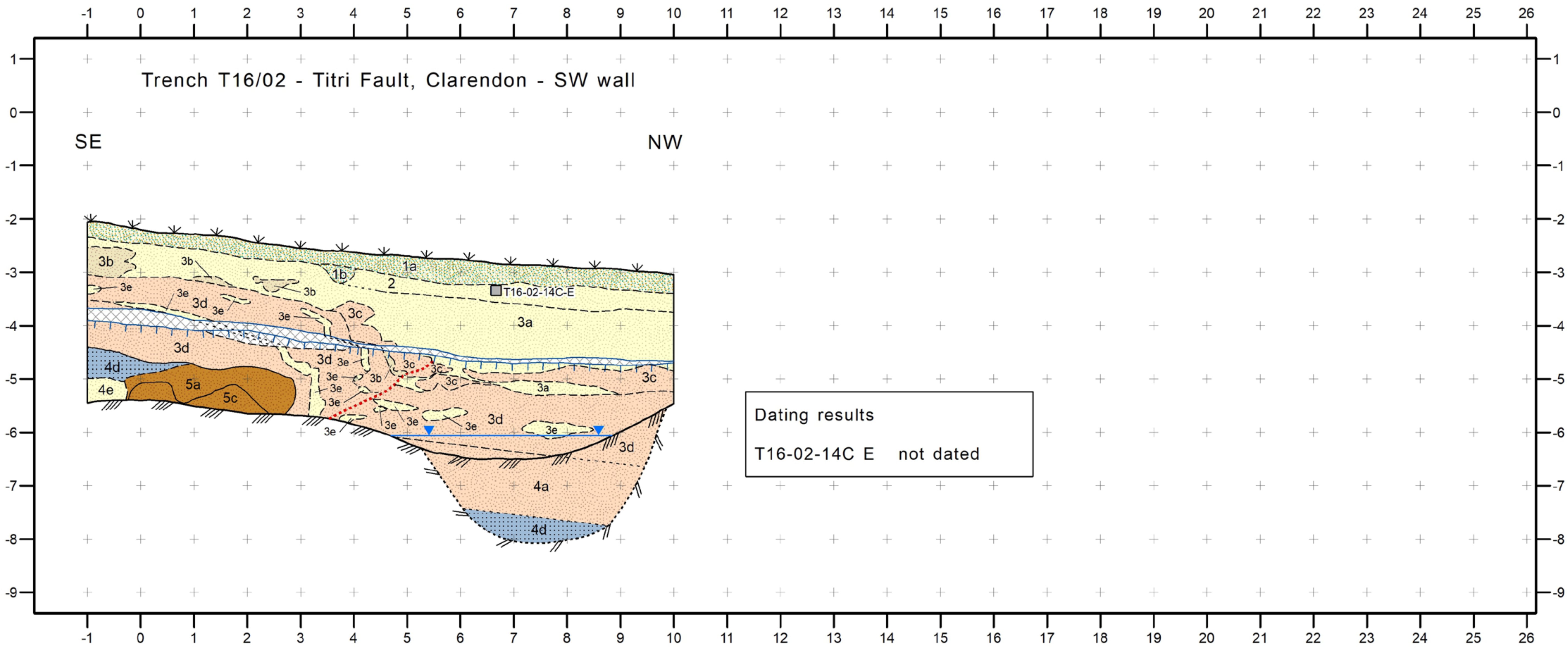

Material descriptions

- Trench spoil
- 1a Grey-brown organic silt
- 2 Light grey to light yellow-brown mottled, massive silt
- 3a Mottled grey to light yellow-orange, massive silt with scattered angular fine gravel stringers and lenses
- 3b Yellow-grey to yellow-brown, fine gravelly sandy silt to sandy silty fine gravel. Gravel clasts typically <3 cm
- 3c Yellow-grey to yellow-brown, subangular to subrounded, silty sandy gravel. Gravel clasts <7 cm
- 3d As for 3c but stratigraphically lower and coarser, with clast size typically 5-8 cm
- 3e Light yellow-grey medium sandy silt lenses or pods in unit 3d
- 3f As for unit 3d, but commonly with orange-brown colour
- 4a As for unit 3d
- 4d Mottled olive to blue-grey clay, with abundant dark organic flecks
- 4e Mottled olive-brown to blue-grey silty very fine sand
- 5a Light grey to dark brown-yellow, stiff-hard, silt, with rare quartz pebbles
- 5c Light grey to dark brown-yellow mottled, stiff, very fine sandy silt with bands, veins and pods of iron oxide

Figure 3.22 Log of Trench T16/02, south-western wall. Log axes are in metres. Minor discontinuous units within a more extensive unit are labelled in smaller font.

Table 3.4 Clarendon trench T16/02 fault displacement information. The values have been estimated from the trench logs (Figures 3.20, 3.21, and 3.22). Fault dip values differ from fault attitudes on the logs that were measured in the field on localised sectors of the fault planes.

Geological Feature	Fault Dip (degrees)			Vertical Separation (m)			Dip-slip Displacement (m)			Estimated Number of Surface-Rupture Events	Average Dip-Slip Single-Event Displacement (m)	
	average	minimum	maximum	median	minimum	maximum	average	minimum	maximum		minimum	maximum
Top of unit 4d (NE & SW walls)	33°	26°	40°	3.3	3.0	3.5	6.1	4.7	8.0	≥2	-	4.0
Top of unit 3d (NE wall)				2.1	1.2	3.0	3.9	1.9	6.7	≥1	-	6.7
Top of unit 3d (SW wall)				2.3	2.2	2.3	4.2	3.4	5.2	≥1	-	5.2
Top of unit 3d as measured along the fault plane (NE wall)	-	-	-	-	-	-	-	~1.0	-	≥1	-	-
Unit 3b (hanging-wall side of fault, NE wall)	-	-	40°	-	0.8	-	-	1.2	-	≥1	-	-

NOTES

Fault dip values were estimated from the logs using a protractor. Four representative estimates were taken over the basal one metre of the logged trench wall, one each on the north-western and south-eastern sides of the fault zone, in each wall. The maximum dip is the steepest value, the minimum dip is the gentlest value, and the average is of all four values. These fault dip values are applied to the vertical separations of each of the geological features listed in the table, irrespective of what localised dip(s) the fault(s) may have at the location of the feature.

Vertical separation of each geological feature across the fault zone is taken from the logs, and includes representative estimates of maximum and minimum separation, based on plausible options for projection of each geological feature into the fault zone (see text for additional information). The median value is midway between the minimum and maximum.

Dip-slip displacement is calculated from the fault dip and vertical separation. The average value is based on the average fault dip and median vertical separation, the maximum value uses the maximum fault dip and minimum separation, and the minimum value comes from maximum fault dip and minimum vertical separation.

The estimated numbers of single-event displacement events refer to the number of surface ruptures that produced the vertical separation of each geological feature and are discussed further in the text.

The dip-slip single-event displacement is the dip-slip displacement value divided by the number of single-event displacements. The minimum value is based on the minimum displacement and larger estimate of events, while the maximum value comes from the maximum displacement and smaller estimate of events.

3.2.3.1 Assessment of fault deformation

Trench T16/02 revealed a single fault with reverse sense of displacement that is sharp in the north-eastern wall (Figure 3.19A), compared with that in the south-western wall (Figure 3.14) where the deformation is almost entirely by buckling with very little discrete fault offset (Figure 3.19B). The buckling is mainly restricted to unit group 3 sandy silt lenses close to the fault. The dip of the fault in the north-eastern wall is relatively shallow (26°) to the southeast.

An important finding of this trench is that only a single rupture event appears to be recorded directly in the trench wall stratigraphy, but differences in gravel thickness either side of the fault indicate earlier event(s). The single rupture event is recorded by the fault displacement and buckling of unit group 3; no colluvial wedge units were identified in this trench. The relative difference in height of the top of unit 4d either side of the fault is ~3 m, whereas the relative height difference, due to a combination of fault deformation and buckling, within the group 3 units is ~1 m (Figure 3.20; Table 3.4). This indicates that the older units have experienced more deformation than the younger ones and is the basis on which groups 3 and 4 were differentiated in this trench.

Three geological features are considered significantly distinctive across the fault to provide useful estimates of fault displacements. They are listed in Table 3.4 and described below. The features referred to can be seen in the trench logs (Figure 3.20, Figure 3.21, Figure 3.22).

Top of unit 4d (NE and SW walls): unit 4d was exposed in a pit on the downthrown side of the fault and laps out northwest onto bedrock on the upthrown side, so cannot be traced all the way to the fault. Nevertheless, taking the relative height of the top of unit 4d in the test pit on the downthrown side of the fault (-7.7 to -7.4 m) and the relative height of the top of unit 4d between ~5 to 18 m on the upthrown side of the fault (-4.2 to -4.4 m), we can calculate a vertical separation of 3 to 3.5 m.

Top of unit 3d (NE and SW walls): unit 3d is buckled close to the fault, but the top of the unit at the far end of the trench on the downthrown side is -5.0 to -5.5 m (SW wall) and -5.2 to -5.3 m (NE wall), and the top at the far end of the trench on the upthrown side is -2.5 to -3.8 m (NE wall) and -3.0 m (SW wall), so the vertical separation across the fault is 1.2 to 3.0 m (NE wall) and 2.2 to 2.3 m (SW wall) (Table 3.4). Measurement of the separation of this contact along the fault provides a minimum estimate of rupture displacement because it does not take account of any of the buckling of the units, of ~1.0 m.

Unit 3b: On the hanging-wall side of fault (NE wall) at least 0.8 m of vertical buckling has deformed unit 3b, and this is regarded as a minimum estimate of vertical separation.

Single event displacements (SED) were calculated from the calculated dip-slip displacement values divided by the number of events as for the other trench sites (Table 3.4). These range from 4.0 to 6.7 m, but they are all considered to be maximum values because the estimated number of events may be a minimum. Given this we take the smallest value, 4.0 m as the preferred maximum single event displacement at the Clarendon T16/02 trench site.

3.2.3.2 Assessment of timing of deformation events

Two OSL ages and one radiocarbon age were obtained from this trench (Table 3.2). OSL sample T16-02-OSL A, collected from unit 4e (Figures 3.20 and 3.23B), was analysed using both the MAAD and SAR methods (Appendix 1), and yielded ages of 75.3 ± 9.5 ka (MAAD) and 70.6 ± 3.4 ka (SAR). The MAAD age has a large uncertainty, and the more precise SAR age is regarded as the more representative age for this unit. Its older bound (i.e. ~74 ka) provides a maximum age for the occurrence of at least two surface rupture events of the Titri Fault at this location.

A sample of organic matter (T16-02-14C B) from overlying unit 4b (Figure 3.21 and Figure 3.23B) was radiocarbon dated and returned an infinite age (i.e. beyond the reach of the radiocarbon technique) of greater than ~45 ka. While not a discrete age, it is compatible with the OSL ages for the underlying unit 4e.

OSL sample T16-02-OSL E was collected from the base of unit 2 and returned an age of 20.0 ± 1.7 ka. This sample was collected just above the fault tip in the north-eastern wall (Figure 3.20) from an un-faulted unit. The younger age bound (i.e. 18.3 ka) provides a minimum age for the most recent surface rupture event at this location.

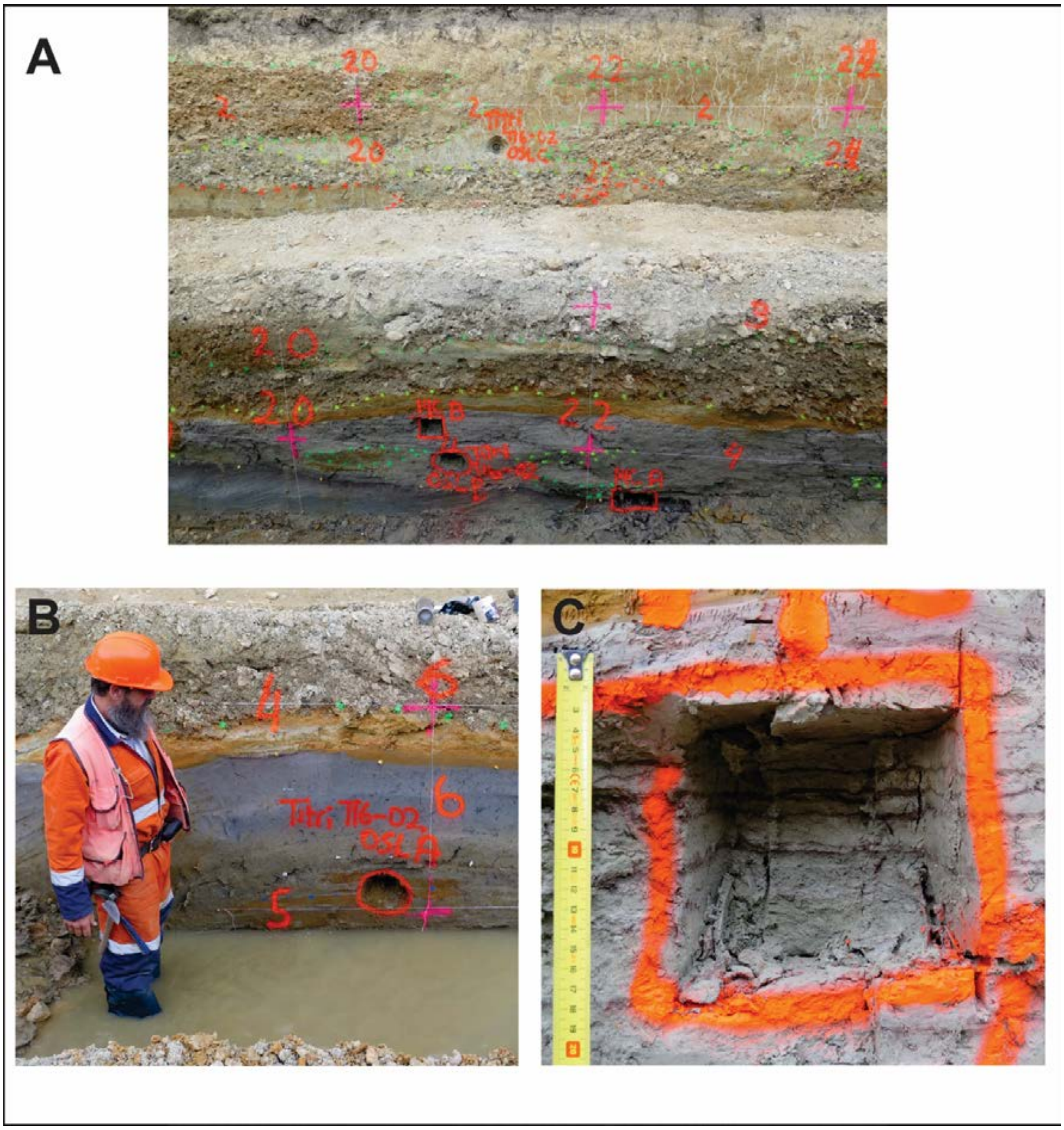

Figure 3.23 Views of sample sites in trench T16/02. A: A view of some of the sampling sites in the north-eastern wall of the trench (see Figure 3.21). Sample 14C B (meterage 21 horizontal, -4 vertical) contained the largest amount of organic material and was selected for radiocarbon dating. B: Location of sample T16-02-OSL A (meterage 5.8 horizontal, -5 vertical; Figure 3.20), collected from unit 4e, beneath the distinctive blue-grey clay layer (unit 4d). Note the dark flecks of organic matter in unit 4d. C: Close-up of sample site T16-02-OSL B in unit 4b, with brown organic-rich layers near the top. A block sample was collected and sieved in the laboratory to obtain solid fragments of organic matter, which were then radiocarbon dated. All photos: GNS Science, D.J.A Barrell.

4.0 TITRI FAULT SURFACE RUPTURE CHARACTERISATION

4.1 Chronology of Surface Rupture Events

The OSL age constraints for the timing and number of ground-surface rupture events at each of the trench sites are summarised in Figure 4.1. At least two events were identified in each trench and the available age constraints show that each of these distinctive and unequivocal events could have occurred simultaneously at each site. As the Glenledi Road and Clarendon localities are only ~8 km apart and are regarded as being on the same segment of the Titri Fault (see below), the following discussion assumes that the same fault rupture events are represented at both localities. We therefore look collectively at the dating-constrained rupture events from all three trenches to place limits on rupture event timing.

In the Clarendon T16/03 trench, an OSL age was obtained for a unit that has only been faulted once (T16-03 - OSL D; marked with an * in Figure 4.1). Assuming this event was the most recent event (MRE), then its timing can be constrained from the older bound of this age and the younger bound of the oldest un-faulted age obtained from the trenches (Clarendon; T16-02 - OSL E) to between 31.3 ka and 18.3 ka.

The penultimate event (PE) can also be constrained from the age of the same unit that has only been faulted once in the Clarendon T16/03 trench (T16-03 - OSL D), and the youngest age from strata that have been faulted at least twice (Glenledi Road; T16-01 - OSL B; SAR age). The older bound of the age of T16-01 - OSL B and the younger bound of the age of T16-03 - OSL D constrain the PE to between 37.9 ka and 27.5 ka.

An earlier rupture (3rd event) is likely represented in the Glenledi Road trench stratigraphy. As discussed in section 3.1, it is regarded as equally possible that the age of Glenledi Road sample T16-01 - OSL B (SAR) is a maximum for that earlier rupture or is a minimum for that rupture. That interpretation is based purely on Glenledi Road trench stratigraphy but can be further informed by consideration of total amounts of dip-slip deformation in each trench, applying the assumption that the same rupture events are represented at both the Glenledi Road and Clarendon localities. At the Glenledi Road trench, dip-slip deformation of between 5.0 and 8.1 m was accrued in at least 2, probably 3 and possibly 4 ruptures (Table 3.1). At Clarendon trench T16/02, between 4.7 and 8.0 m of dip-slip deformation accrued from at least two ruptures that occurred sometime after deposition of units 4d and 4e (Table 3.4). We therefore infer that the earlier rupture at Glenledi Road is also represented in the stratigraphy of Clarendon trench T16/02. On that basis, the older age bound of sample T16-02 – OSL A; SAR age, from unit 4e in Clarendon trench T16/02 (74.1 ka), provides a maximum age for the likely earlier event at Glenledi Road.

That interpretation for the 3rd event, and the MRE and PE set out above, comprises scenario 1 of Figure 4.1. However, as discussed in section 3.1 the uncertainty both with regards to the number of rupture events exposed in the Glenledi Road trench (Figures 3.2 and 3.4) and the timing of those events, leads us to identify scenarios 2 and 3 of Figure 4.1. Scenario 2 illustrates the possibility that the older bound of the age of T16-01 - OSL B is a maximum for the 3rd rupture event. Scenario 3 highlights a possible additional event, which is based on indirect and speculative evidence from the Glenledi Road trench. Scenario 1 is our preferred rupture timing interpretation for the sector of the Titri Fault investigated in this study, because it has a more firmly established maximum age for the observed deformation. Scenario 3 is our least preferred interpretation, because it includes a rupture event of questionable recognition.

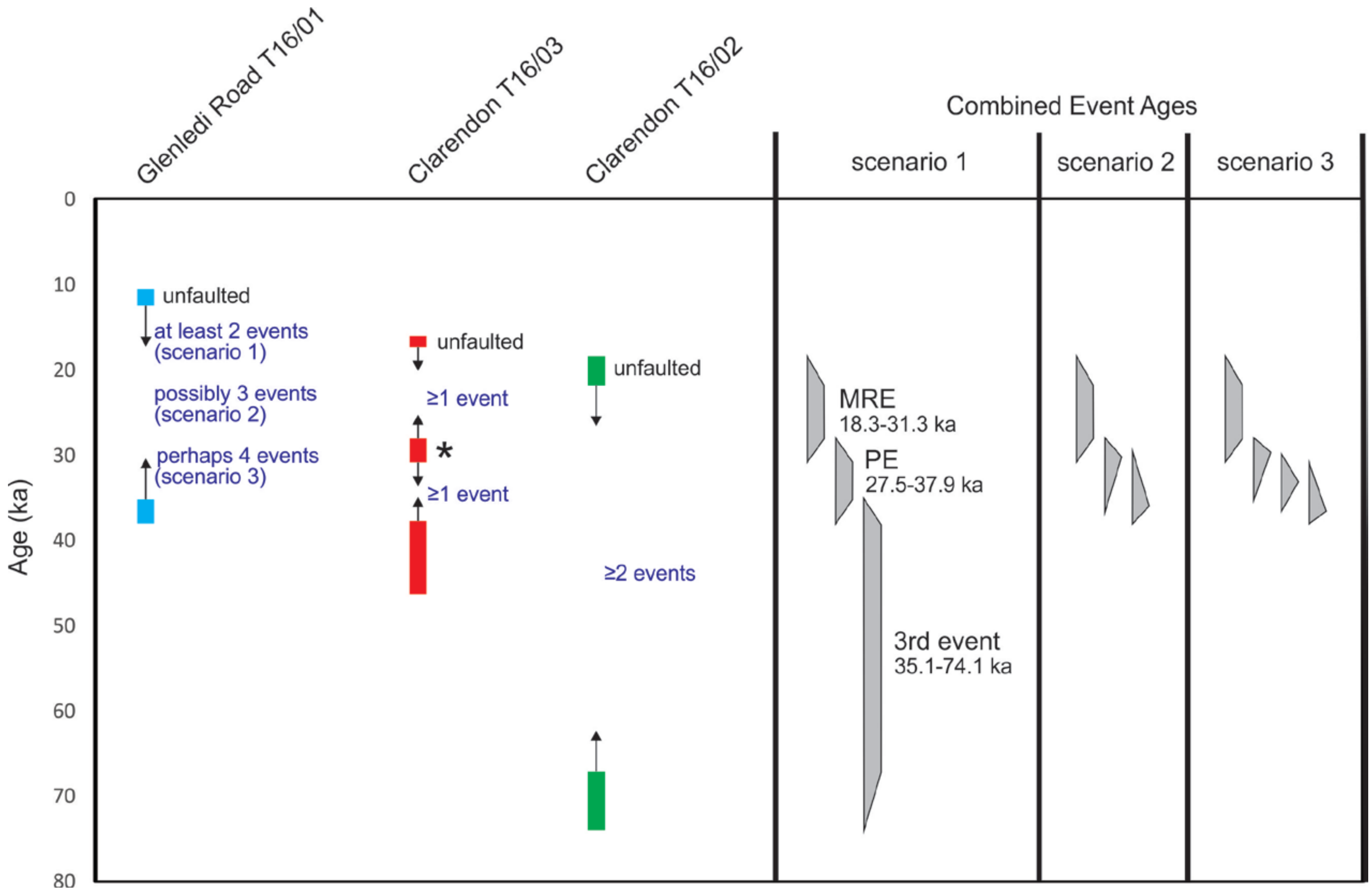

Figure 4.1 OSL age constraints for the timing of rupture events on the Titri Fault from this study. The grey trapezoids/triangles on the right-hand side depict the timings of individual ruptures under three different rupture timing scenarios adopting combined event records, assuming each rupture occurred at both the Glenledi Road and Clarendon localities. MRE = most recent event, PE = penultimate event.

4.2 Recurrence Interval

It is challenging to come up with a robust estimate of recurrence interval given the small number of events interpreted from the Titri Fault trenches, and the uncertainty surrounding both the number and ages of those events. However, with reference to Figure 4.1, some indicative recurrence interval ranges can be derived. One rupture timing scenario (scenario 1; based on option 1 from the Glenledi Road trench interpretation) has two rupture events, with the earlier one (PE) occurring sometime between 27.5 to 37.9 ka. This yields an average recurrence interval in the range of 14 to 19 ky[3]. Scenario 2 acknowledges a possibility that three surface rupture events have occurred, with the earliest sometime between 27.5 to 37.9 ka. Scenario 3 accommodates the possibility of an additional rupture event within the same amount of time as scenario 2. Scenarios 2 and 3 imply average recurrence intervals respectively in the range of 9 to 13 ky and 7 to 9 ky.

The trenching results show that at least 18,300 years have elapsed since the most recent surface rupture. This means that scenario 1 allows the possibility that surface ruptures have been spaced regularly through time, whereas scenarios 2 and 3 require an episode of relatively frequent ruptures prior to 18.3 ka, with quiescence since then.

Based on the above, it would appear that since ~38 ka, the recurrence interval of the central section of the Titri Fault can be poorly constrained to between ~7,000 and ~19,000 years. Acknowledging our greater preference for scenario 1 and least preference for scenario 3, we give more weight to the longer part of that recurrence interval range.

4.3 Single Event Displacement

We summarise the single event displacement (SED) estimates from each trench in Table 4.1. They are dip-slip SEDs but, because we have found no evidence for strike-slip displacement, we interpret them to also be net slip SEDs.

The largest minimum and the smallest maximum SED estimates from the Glenledi Road trench are 1.3 m and 2.7 m, respectively. At the Clarendon locality the largest minimum and the smallest maximum SED estimates are 2.4 m (average between both walls) and 4.0 m, respectively. Following from the assumption that previous ruptures are represented at both the Glenledi Road and Clarendon localities (section 4.1), we consider it appropriate to constrain the SED to between the smallest maximum and the largest minimum estimates, placing it in the range of 2.4 to 2.7 m. The middle of that range (2.6 m, with rounding) is our best estimate of average SED for this sector of the Titri Fault.

Table 4.1 Summary of net single-event displacement estimated for each trench site. For further details see Tables 3.1, 3.3 and 3.4 and the accompanying text.

Trench	Number of events	Minimum (m)	Maximum (m)
Glenledi Road T16/01	≥4	1.3	2.7
Clarendon T16/03	2	2.4	
Clarendon T16/02	≥1		4.0

[3] 1 ky = an interval of 1000 years

4.4 Slip Rate

We calculate slip rate from the oldest dated units in each trench as summarised in Table 4.2. Where possible, the minimum and maximum values are calculated by dividing the minimum displacement by the maximum age, and by dividing the maximum displacement by the minimum age, respectively. For calculation, we employ the older bound of uncertainty for maximum ages and the younger bound of uncertainty for minimum ages. These are dip-slip rates that we regard as net slip rates because there is no evidence for strike-slip displacement.

For the Glenledi Road trench we calculate two slip rates. One is from the contact between unit groups 4 and 3 and the other is from the contact between unit groups 5 and 4. These are both constrained by the same age determination, from the upper part of unit group 4 (sample T16-01 - OSL B, SAR age; 36.5 ± 1.4 ka). This age determination is a minimum for the age of the underlying unit 5/4 contact and so the derived slip rate of 0.08 mm/yr is considered a minimum. Similarly, that sample affords a maximum age for the overlying unit 4/3 contact and the slip rate of 0.23 mm/yr derived from that contact is considered a maximum.

For the Clarendon T16/03 trench the unit 4/3 contact age is constrained by two age determinations, one from within unit 4 (T16-03 - OSL A; 42.0 ± 4.3 ka) and one from within unit 3 (T16-03 - OSL D; 29.4 ± 1.9 ka). The dip-slip displacement of that contact (4.7 m) is regarded as a minimum value because the top of unit 4 may have been eroded in the hanging wall, and furthermore we use an average of calculated dip-slip displacements from each wall (4.5 and 4.9 m). We use the displacement value together with the older bound of the maximum age to calculate a minimum estimate of slip rate of 0.10 mm/yr.

For the Clarendon T16/02 trench, sample T16-02 - OSL A from within unit group 4 provides a maximum age of 70.6 ± 3.5 ka for the unit 4/3 contact. The older bound of that age determination together with the minimum displacement estimate provide a minimum estimate of slip rate of 0.06 mm/yr.

Table 4.2 Net slip rates from displacements of the older age-constrained geological features in each trench.

Trench	Contact	Dip-slip displacement (m)			Age (ka)			Slip rate (mm/yr)		
		Ave.	Min.	Max.	Ave.	Min.	Max.	Ave.	Min.	Max.
Glenledi Road T16/01	4/3	3.9	3.1	5.6	36.5	35.1	37.9		0.08	
Glenledi Road T16/01	5/4			8.1	36.5	35.1	37.9			0.23
Clarendon T16/03	4/3		4.7		29.4	27.5	31.3		0.10	
Clarendon T16/02	4/3	6.1	4.7	8.0	70.6	67.1	74.1		0.06	

The range of slip rates calculated are 0.08–0.23 mm/yr. Taking the largest minimum estimate and the only maximum estimate, and rounding to the nearest 1 decimal place, we assess the slip rate for the Titri Fault in the Clarendon to Milton area as being in the range of 0.1 to 0.2 mm/yr.

5.0 DISCUSSION

5.1 Comparison with Previous Studies and Nearby Sites

The results of this study show that the Titri Fault is an active fault, as defined by having experienced surface-rupture activity since 125 ka (Langridge et al. 2016), and that it is more active than previously thought (Litchfield 2001; Litchfield and Lian, 2004). The MRE on the Titri Fault occurred sometime between 18.3 and 31.3 ka and the PE occurred sometime between 27.5 and 39.7 ka. This contrasts with the previous inferences of no activity since the middle of the last glaciation (~50 ka) and no substantial activity since at least ~125 ka (Litchfield 2001) and a later assessment based on indirect OSL dating evidence of no activity since ~92 ka (Litchfield and Lian 2004). However, the new findings are consistent with evidence of no activity in the Holocene as concluded by Litchfield (2001).

Parallel to and ~10 km east of the Titri Fault is the Akatore Fault (Figure 1.1), which has also recently been shown to be more active than previously thought (Taylor-Silva et al. 2020). Trenches at two sites on the central and southern Akatore Fault showed that its MRE occurred between 0.7 and 0.9 ka, its PE between 1.0 and 1.2 ka and its previous event (antepenultimate, APE) sometime between 1.3 and 15.3 ka. Prior to the APE, there appear to have been no surface rupture events on the Akatore Fault at least as far back as 125 ka. The three most recent events on the Akatore Fault post-date the MRE on the Titri Fault and conversely, the Titri Fault events from this study occurred during the period of no surface-rupture earthquakes on the Akatore Fault. This potential anti-correlation is explored further in the next section.

5.2 Episodicity and Earthquake Clustering

A secondary aim of this study, contingent upon what the trenching and dating found, was to investigate whether ruptures of the Titri Fault have been clustered in time. Earthquake clustering refers to periods of time with frequent earthquakes separated by relatively long periods of time with few or no earthquakes, which is also referred to as episodic activity (e.g. Berryman and Beanland 1991). Episodic activity appears to occur particularly in areas of relatively low strain rate, such as Australia (e.g. Clark et al. 2012) and has been suggested for several faults in Otago (Beanland et al. 1986; Beanland and Berryman 1989; Litchfield and Norris, 2000; Norris and Nicolls 2004; Griffin et al. 2019; Taylor-Silva et al. 2020). Documenting episodic activity is important (and challenging) for earthquake hazard as it is important to know if a fault is in an active or quiet period, and to get an indication of how long the episodes of activity (or quiescence) may last.

The results of this study provide hints, but not definitive evidence, of episodic activity on the Titri Fault. Based on our preferred rupture timing scenario (scenario 1; Figure 4.1) there have been no surface rupturing earthquakes on the south-central sector of the Titri Fault since at least~18.3 ka. However, in the ~20 ky interval before that there were at least two surface ruptures, and perhaps as many as four (Figure 4.1). This suggests that the Titri Fault may have had clustered earthquakes during the period ~18 to 38 ka, but none thereafter. However, if only two events occurred during that time interval, they need not have been clustered.

Regardless of the exact number of events that occurred, the results of this study conclusively show that the Titri Fault was active in the period ~18–38 ka, which is a period of no activity on the nearby Akatore Fault (Taylor-Silva et al. 2020). This provides evidence to support previous interpretations that the central and east Otago faults are linked at depth and that the relatively low overall strain rate is distributed unevenly across the fault and fold system, being localised on a few faults at a time. The possible anti-correlation of events further hints that potentially when one fault switches on, a nearby fault switches off. Work is in progress to investigate episodic activity through trenching studies of several other central and east Otago faults (e.g. Griffin et al. 2019).

5.3 Implications for Seismic Hazard Modelling

The Titri Fault was not included in the 2010 version of the New Zealand National Seismic Hazard Model (NSHM; Stirling et al. 2012) because previous work showed only marginal evidence for activity since at least 125 ka (Litchfield 2001; Litchfield and Lian 2004). The results of this study show that it clearly is an active fault, by the definition in Langridge et al. (2016), and despite the possible evidence that it is currently less active than in the period ~18 to 38 ka, it is prudent to now include it as an earthquake (fault) source in the NSHM as has been done for other central and coastal Otago faults. The Titri Fault and has been included in some recent seismic hazard studies (summarised by Villamor et al. 2018) and will be included in the current revision of the NSHM. We do not repeat the details of the seismic hazard studies, but briefly summarise the Titri Fault geometry and parameters that have been used in recent seismic hazard studies and should be considered in future ones.

Together with the results of this study, previous interpretations that the Titri Fault is segmented (Litchfield 2001), mapping showing the continuation of the north end of the Titri Fault as an anticline (Villamor et al. 2018), and new mapping using lidar showing likely continuity of deformation along the Castle Hill Fault to the south (Barrell 2020) provide a basis for re-evaluation of Titri Fault seismic hazard. Villamor et al. (2018) modelled the Titri Fault as comprising three ~30 km long fault sources (segments) as shown in Figure 5.1. They are named for simplicity Titri North, Titri Central, and Titri South. Under this seismic source delineation, both the Glenledi Road and Clarendon trench sites are on the same, Titri Central, earthquake fault source, which is compatible with our inference that at least two of the most recent earthquakes on the fault ruptured both localities. The dip of the Titri Fault in the trenches ranges from 24° to 67° SE and we infer an overall dip of 45°, a value that has been applied to most other Otago faults in the NSHM (Stirling et al. 2012). Based on the results of our investigation along the central segment of the Titri Fault, we suggest the following parameter value ranges be used for this segment of fault in future seismic hazard evaluations: slip rate 0.1 to 0.2 mm/yr; SED 2.4 to 2.7 m; and recurrence interval ~7 to 19 ky with a preference towards the longer end of that range (e.g. 14 to 19 ky).

Titri Fault parameters and results from recent seismic hazard studies summarised by Villamor et al. (2018) were informed by preliminary results of this study and are shown in Table 5.1. These show that the Titri Fault is modelled as being capable of producing earthquakes of between magnitude 7.0 and 7.7, and that two-segment and whole fault ruptures are modelled as having longer recurrence intervals than single segment ruptures. A whole-fault rupture (model 3; Table 5.1) has a recurrence interval about 4 times longer than a single segment rupture (model 1; Table 5.1). The SED values obtained from our trenching-based investigations for the most recent surface-rupture earthquakes are more compatible with a one- or two-segment rupture scenario, because the SEDs would likely be much larger had they been produced by a whole-fault rupture. It should be noted that the slip rates applied to the Titri Fault by Villamor et al. (2018) are somewhat larger than the values used in this report, and the recurrence intervals calculated by Villamor et al. (2018) may need to be reassessed.

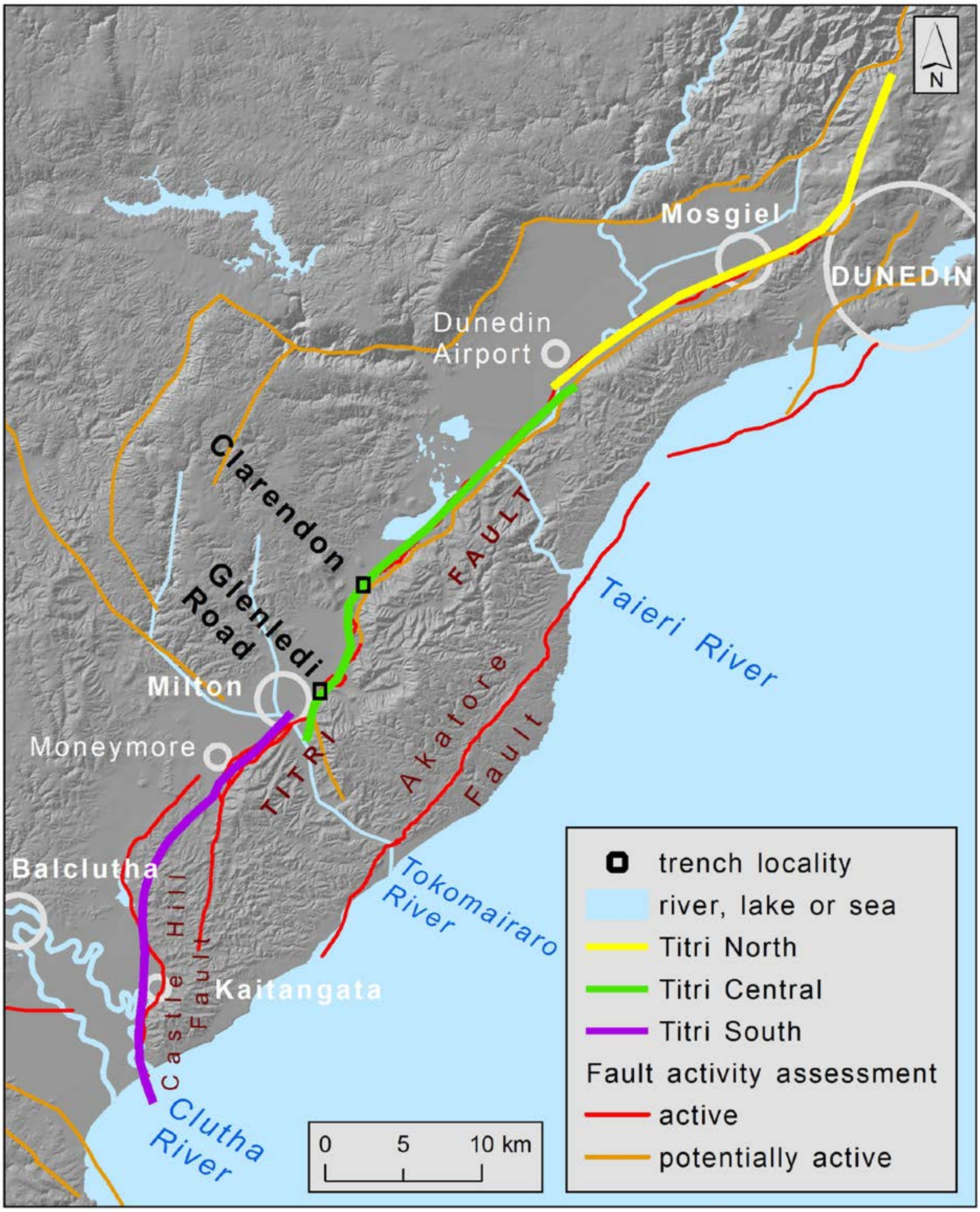

Figure 5.1 Titri Fault segment sources for seismic hazard modelling purposes.. The distribution of active and potentially active faults is from Barrell (2020).

Table 5.1 Titri Fault alternative fault rupture scenarios, and fault dip and length estimates used to calculate earthquake magnitudes, from Villamor et al. (2018).

Model	Fault source	Dip (°)	Length (km)	Magnitude (Mw)
1 – single faults	Titri North	45	29	7.0
	Titri Central	45	30	7.0
	Titri South	45	29	7.0
2 – 2 faults combined	Titri North-Central	45	59	7.4
	Titri Central - South	45	59	7.4
3 – all faults combined	Titri All	45	98	7.7

One way to test the potential for two segment, or entire fault rupture, would be to undertake trenching and dating studies at sites on the North and South segments. The South segment in particular looks prospective as there are prominent scarps near Moneymore (Figure 5.1).

6.0 CONCLUSIONS

Three trenches excavated across the central part of the Titri Fault at two localities about 8 km apart have shown that:

- The Titri Fault is an active fault that has experienced surface rupturing earthquakes within the past 125,000 years.
- The sense of movement is reverse, upthrown to the southeast, and observed surface fault dips range from 24° to 67° SE.
- Evidence for at least two ground-surface rupturing earthquake events was documented in all three trenches.
- Seven Optically Stimulated Luminescence (OSL) ages and one radiocarbon age showed that two events could have been the same at all three trench sites.
- Assuming this to be the case then the most recent event (MRE) occurred between 18.3 and 31.3 ka and the penultimate event (PE) between 27.5 and 37.9 ka.
- An earlier, likely, event, and another possible but unlikely event, are poorly dated. The likely earlier event is assessed as having occurred more recently than ~74,000 years ago and could possibly have occurred in the time interval between 28-37.9 ka.
- Recurrence interval, calculated by dividing the time interval spanned by the earthquakes by the number of events, ranges between ~7,000 and ~19,000 years, with a preferred value being weighted towards the longer end of that range.
- Single event displacement (SED), calculated by dividing dip-slip displacements by the number of events, is constrained to a range of 2.4 to 2.7 m. There is no evidence for strike-slip motion at the trench sites, so this is considered to be a net SED.
- Slip rate, calculated by dividing the dip-slip rate displacement of the oldest dated units in the trench by their age is in the range of 0.1 to 0.2 mm/yr. The lack of evidence for strike-slip motion means this rate is considered to be a net slip rate.
- The Titri Fault events occurred during a time interval of no events on the nearby Akatore Fault. The data for the Titri Fault does not resolve whether or not its recent ruptures were clustered in time.
- The Titri Fault should be included in the NSHM, and seismic hazard modelling undertaken to date suggests that the Titri Fault could produce earthquakes in the range of magnitude 7.0 to 7.7.
- There is potential to test the clustering and segmented fault source characterisation by dating more of the OSL samples collected in 2016, or by trenching and dating investigations at other sites, such as prominent scarps near Moneymore on the southern segment.

7.0 ACKNOWLEDGMENTS

This work was funded by the Earthquake Commission under their Biennial Contestable Grants Programme, “Earthquake hazard in Dunedin: paleoseismology of the Titri Fault (Project No 16/719)”. We express our gratitude to the Fegan family (Glenledi Road) and the Copland family (Clarendon) for readily allowing access to their land. We thank Keith McLeod of Keith McLeod Excavation Limited for constructing and restoring three excellent trenches, and Jenny Dahl of the GNS Science Rafter Radiocarbon Laboratory for the painstaking sieving and analysis of the radiocarbon sample. Belinda Smith Lyttle did an excellent job of digitising the trench logs. We thank Rob Langridge and Dougal Townsend for reviewing the report.

8.0 REFERENCES

Barrell DJA. Forthcoming 2020. General distribution and characteristics of active faults and folds in the Clutha and Dunedin City districts, Otago. Dunedin (NZ): GNS Science. (GNS Science consultancy report 2020/88). Prepared for Otago Regional Council.

Barrell DJA, Forsyth PJ, Litchfield NJ, Brown LJ. 1999. Quaternary stratigraphy of the Lower Taieri Plain, Otago, New Zealand. Lower Hutt (NZ): Institute of Geological & Nuclear Sciences. 24 p. (Institute of Geological & Nuclear Sciences science report; 99/15).

Barrell DJA, McIntosh PD, Forsyth PJ, Litchfield NJ, Eden DN, Glassey PJ, Brown LJ, Froggatt PC, Morrison B, Smith Lyttle B, et al. 1998. Quaternary fans and terraces of coastal Otago. Lower Hutt (NZ): Institute of Geological & Nuclear Sciences. 36 p. (Institute of Geological & Nuclear Sciences science report; 98/11).

Barrell DJA, Read SAL, Van Dissen RJ, Macfarlane DF, Walker J, Rieser U. 2009. Aviemore: a dam of two halves. In: Turnbull IM, editor. Geological Society of New Zealand & New Zealand Geophysical Society Joint Annual Conference, Oamaru, 23–27 November 2009: field trip guides. Wellington (NZ): Geological Society of New Zealand. 30 p.

Beanland S, Berryman KR. 1989. Style and episodicity of late Quaternary activity on the Pisa-Grandview Fault Zone, Central Otago, New Zealand. *New Zealand Journal of Geology and Geophysics*. 32(4):451–461. doi:10.1080/00288306.1989.10427553.

Beanland S, Berryman KR, Hull AG, Wood PR. 1986. Late Quaternary deformation at the Dunstan fault, Central Otago, New Zealand. In: *Recent crustal movements of the Pacific region*. Wellington (NZ): Royal Society of New Zealand. p. 293–306. (Royal Society of New Zealand bulletin; 24).

Benson WN. 1968. The W.N. Benson geological map of Dunedin district [map]. Wellington (NZ): Department of Scientific and Industrial Research. 1 folded map + 1 booklet, scale 1:50,000. (Miscellaneous series map / New Zealand Geological Survey; 1).

Berryman KR, Beanland S. 1991. Variation in fault behaviour in different tectonic provinces of New Zealand. *Journal of Structural Geology*. 13(2):177–189. doi:10.1016/0191-8141(91)90065-q.

Bishop DG. 1994. Geology of the Milton area: sheets H45BD & part I45 [map]. Lower Hutt (NZ): Institute of Geological & Nuclear Sciences. 1 folded map + 32 p., scale 1:50,000. (Institute of Geological & Nuclear Sciences geological map; 9).

Bishop DG, Turnbull IM. 1996. Geology of the Dunedin area [map]. Lower Hutt (NZ): Institute of Geological & Nuclear Sciences. 1 folded map + 52 p., scale 1:250,000. (Institute of Geological & Nuclear Sciences 1:250,000 geological map; 21).

Clark D, McPherson A, Van Dissen RJ. 2012. Long-term behaviour of Australian Stable Continental Region (SCR) faults. *Tectonophysics*. 566–567:1–30. doi:10.1016/j.tecto.2012.07.004.

Edbrooke SW, Heron DW, Forsyth PJ, Jongens R. 2014. Geological map of New Zealand 1:1,000,000: digital vector data 2014. Lower Hutt (NZ): GNS Science. 1 DVD-ROM. (GNS Science geological map; 2).

Griffin J, Stirling MW, van den Berg E, Barrell DJA, Nicolls R, Todd E, Wang N. 2019. Paleoseismology of the Hyde Fault and implications for episodic fault activity in the Otago range and basin province [abstract]. In: Kamp PJJ, Pittari A, editors. *Abstract volume: Geosciences 2019, 24–27 November 2019, Hamilton*; Wellington (NZ): Geoscience Society of New Zealand. p. 71. (Geoscience Society of New Zealand miscellaneous publication; 155A).

Heron DW, custodian. 2018. Geological map of New Zealand 1:250,000. 2nd ed. Lower Hutt (NZ): GNS Science. 1 USB. (GNS Science geological map; 1).

Harrington HJ. 1958. Geology of Kaitangata Coalfield. Wellington (NZ): Department of Scientific and Industrial Research. 2 vol. (New Zealand Geological Survey bulletin; 59).

Langridge RM, Ries WF, Litchfield NJ, Villamor P, Van Dissen RJ, Barrell DJA, Rattenbury MS, Heron DW, Haubrock S, Townsend DB, et al. 2016. The New Zealand Active Faults Database. *New Zealand Journal of Geology and Geophysics*. 59(1):86–96. doi:10.1080/00288306.2015.1112818.

Litchfield NJ. 2000. Quaternary deformation at the leading edge of the Otago reverse fault province [PhD thesis]. Dunedin (NZ): University of Otago. 1 v.

Litchfield NJ. 2001. The Titri Fault System: Quaternary-active faults near the leading edge of the Otago reverse fault province. *New Zealand Journal of Geology and Geophysics*. 44(4):517–534. doi:10.1080/00288306.2001.9514953.

Litchfield NJ, Lian OB. 2004. Luminescence age estimates of Pleistocene marine terrace and alluvial fan sediments associated with tectonic activity along coastal Otago, New Zealand. *New Zealand Journal of Geology and Geophysics*. 47(1):29–37. doi:10.1080/00288306.2004.9515035.

Litchfield NJ, Norris RJ. 2000. Holocene motion on the Akatore Fault, south Otago coast, New Zealand. *New Zealand Journal of Geology and Geophysics*. 43(3):405–418. doi:10.1080/00288306.2000.9514897.

McKellar IC. 1990. Southwest Dunedin urban area [map]. Lower Hutt (NZ): New Zealand Geological Survey. 1 folded map + 1 booklet, scale 1:25,000. (New Zealand Geological Survey miscellaneous series map; 22).

Mutch AR, Wilson DD. 1952. Reversal of movement of the Titri Fault. *New Zealand Journal of Science and Technology B, General Section*. 33(5):398–403.

Norris RJ, Nicolls R. 2004. Strain accumulation and episodicity of fault movements in Otago. Wellington (NZ): Earthquake Commission. 146 p. EQC Research Report 01/445.

Stirling MW, McVerry GH, Gerstenberger MC, Litchfield NJ, Van Dissen RJ, Berryman KR, Barnes P, Wallace LM, Villamor P, Langridge RM, et al. 2012. National seismic hazard model for New Zealand: 2010 update. *Bulletin of the Seismological Society of America*. 102(4):1514–1542. doi:10.1785/0120110170.

Taylor-Silva BI, Stirling MW, Litchfield NJ, Griffin JD, van den Berg EJ, Wang N. 2020. Paleoseismology of the Akatore Fault, Otago, New Zealand. *New Zealand Journal of Geology and Geophysics*. 63(2):151–167. doi:10.1080/00288306.2019.1645706.

Villamor P, Barrell DJA, Gorman A, Davy BW, Hreinsdottir S, Hamling IJ, Stirling MW, Cox SC, Litchfield NJ, Holt A, et al. 2018. Unknown faults under cities. Lower Hutt (NZ): GNS Science. 71 p. (GNS Science miscellaneous series; 124).

This page left intentionally blank.

APPENDICES

This page left intentionally blank.

APPENDIX 1 OSL DATING REPORT

Report No. 7/16

Luminescence Dating Technical Report

Luminescence Dating Laboratory
School of Geography, Environment and Earth Sciences
Victoria University of Wellington
Wellington
New Zealand

Reported by:	Ms. Ningsheng Wang
Date of Issue:	27-09-2016
Contact:	Room 414
	Cotton Building
	Victoria University of Wellington
	Ph: (04) 463 6127

1

CONTENTS

1. **Summary** **3**
2. **Sample Preparation** **3**
3. **Measurements** **4**
4. **Results** **7**
5. **References** **9**

1. SUMMARY

Seven samples (Field code: T16-01-OSL B, T16-01-OSL G,T16-02-OSL A,T16-02-OSL E,T16-03-OSL A,T16-03-OSL D and T16-03-OSL G) were submitted for luminescence dating by David Barrell, GNS Science. The laboratory codes of the samples are WLL1211-WLL1217 respectively.

Due to fine material, fine grain (4-11μm) preparation technique was used. The blue luminescence was measured during infrared stimulation of fine grain feldspar. The luminescence ages were determined by Multiple Aliquot Additive Dose method (MAAD). The ages of WLL1211, WLL1213 and WLL1217 were determined by Single Aliquot Regenerative method (SAR) as well. The dose rate was determined on the basis of gamma spectrometry measurements..

2. SAMPLE PREPARATION

The sample preparation consisted of two parts:

(i) Preparation for measurement of equivalent dose (equivalent to the paleodose)

(ii) Preparation for measurement of dose rate

Part 1: The Preparation for Measurement of Equivalent Dose (D_e)

1. Chemical Treatment

Samples had their outer surfaces removed. Of this removed outer scrapings, 100g was weighed and dried in an oven in preparation for gamma spectrometer analysis.
A plastic cube was then filled with remaining scrapings in preparation for water content measuring.

"Fresh" sample material, that had outer surfaces removed earlier (unexposed light sample material), was treated in 10% HCl. This was carried out overnight until all carbonate was removed by the reaction. Following this treatment the sample was further reacted overnight with 10% H_2O_2 in order to remove organic matter.

The next step involved 200ml CBD* solution being added to the sample for 12 hours to remove iron oxide coatings. Note, after every chemical treatment procedure distilled water was used to wash the sample several times.

*CBD solution: 71g sodium citrate, 8.5 g sodium bicarbonate, and 2g sodium dithionate per litre of distilled water

2. Fine Grain Technique (4-11μm)

After chemical treatment, calgon solution (1g sodium hexametaphosphate per litre distilled water) was added to make thick slurry. This slurry was placed into an ultrasonic bath and mechanically agitated for an hour. The sample was then placed into a 1L measuring cylinder, filled with a certain amount of distilled water to separate out the 4-11μm grains according to Stokes' Law.

The 4-11μm grains were then rinsed with ethanol and acetone and a suspension of these grains were then deposited evenly onto 70 aluminium disks.

Part 2: The Preparation of Measurement of Dose Rate

The dry, ground and homogenised sample material were weighed and sealed in air tight perspex containers and stored for at least four weeks. This storage time minimizes the loss of the short lived noble gas ^{222} Rn and allows ^{226}Ra to reach equilibrium with its daughters ^{214} Pb and ^{214} Bi.

3. MEASUREMENTS

Luminescence age was determined by two factors: the equivalent dose (D_e) and the dose rate.

Equivalent dose: obtained from the lab equivalents to the paleodose absorbed by samples during the burial time in the natural environment since their last exposure to the light.
Dose rate: amount dose received by the sample each year.

Part 1: Determination of Equivalent Dose (D_e)

De was obtained by using MAAD and SAR.

Multiple Aliquot Additive Dose Method (MAAD)

The test dose obtained from an initial test measurement was used for the MAAD. As luminescence vary between disks, all disks for MAAD need to be normalised before β irradiation. Six groups (30 disks divided by five) were β irradiated up to five times of the test dose. Beta irradiation were done on the Riso TL-DA-15 $^{90}Sr/Y$ β irradiator, calibrated against ^{60}Co gamma source, SFU, Vancouver, Canada with about 3% uncertainty. Three groups (three disks per group) were α irradiated up to three times of the test dose. The α irradiation was carried out on a ^{241} Am irradiator, supplied and calibrated by ELSEC Littlemore, UK. The next step was that these 39 disks together with nine non-irradiated disks (total of 48 disks) were stored for four weeks to relax the crystal lattice after irradiation.

After storage, the 48 disks were preheated for five minutes at 230°C, then were measured using a Riso TL-DA-15 reader with infrared diodes at 880nm used to deliver a stimulated beam at 50°C temperature for 100s. Blue luminescence centred about 410nm emission from feldspar was then detected by an EMI 9235QA photomultiplier fixed behind two filters consisting of a Schott BG-39 and Kopp 5-58.

Luminescence growth curve (β induced luminescence intensity versus added dose) was constructed by using the initial the first a few seconds of the shine down curves and subtracting the average of the last 20 seconds, along with the so called late light which was thought to be a mixture of background and hardly bleachable components. Extrapolation of this growth curve to the dose axis was obtained the equivalent dose D_e which was used as a paleodose. This was used to determine the equivalent dose (equivalent to the palaeodos). The shine plateau was checked to be flat after this manipulation.

Measurement of a-value

A similar plot for the alpha irradiated disks allows for an estimation of α efficiency, a-value (a-value is measured by comparing the luminescence induced by alpha irradiation with that induced by beta or gamma irradiation). The a-value was for dose rate calculation.

Single Aliquot Regenerative Method (SAR)

The Single Aliquot Regenerative Method (SAR) was used to determine the equivalent doses. This technique is described by Murray and Wintle (2000).

For the SAR method, a number of aliquots (disks) were subjected to a repetitive cycle of irradiation, preheating and measurement. Firstly, natural shining down curves was measured after preheating. Then shining down curves were measured for the next four or five cycles for different beta doses. Then from the variety of shining down curves, a luminescence growth curve (β induced luminescence versus added dose) was established. This was used to determine the equivalent dose (equivalent to the palaeodose). The measurement for the aliquots resulted in a variety of equivalent doses, so called dose distribution. D_e given in the report were used the arithmetic mean of the data.

In order to correct potential sensitivity changes from cycle to cycle, the luminescence response to a test dose was measured after preheat between cycles.

10 to 12 aliquots of each sample were measured. Preheat and cut heat temperature and time was 250°C for 10 seconds; and measurement time was 100 seconds at 50°C temperature. Luminescence growth curve (β induced luminescence intensity versus added dose) was constructed by using the initial 20 channels (8 seconds) of the shine down curves and subtracting the last 100 channels which was thought to be background. Interpolation of this growth curve to the dose axis was yielded the equivalent dose D_e which was used as a paleodose. The measurements of 10-12 aliquots obtained 10-12 D_e's, the D_e's were accepted within 10% recycling ratio. D_e used for the age determination was used the arithmetic means of the data. A dose recovery test and a zero dose were checked no anomalies.

6

Part 2: Determination of Dose Rate

Dose rate consisted of two parts.

(i) Dose rate from sample's burial environment

(ii) Dose rate from cosmic rays.

(i) *Dose rate from burial environment*

Dose rate from sample's burial environment was determined by radionuclide contents of ^{238}U, ^{232}Th and ^{40}K, a-value and water content.

Determination of Contents of U, Th and K by Gamma spectrometry

Gamma rays produced from sample material was counted for a minimum time of 24 hours by a high resolution and broad energy gamma spectrometer. The spectra were then analysed using GENIE2000 software. The contents of U, Th and K were obtained by comparison with standard samples. The dose rate calculation was based on the activity concentration of the nuclides ^{40}K, ^{208}Tl, ^{212}Pb, ^{228}Ac, ^{214}Bi, ^{214}Pb, ^{226}Ra, using dose rate conversion factors published by Guérin, G., Mercier, N., Adamiec, G. 2011.

Measurement of Water Contents

Water content was measured as weight of water divided by dry weight of the sample taking into account a 5% uncertainty.

(ii) *Dose rate from cosmic rays*

Dose rate from cosmic rays were determined by the depth of sample below the surface along with its longitude, latitude and altitude, convention formula and factors published by Prescott, J.R. & Hutton, J.T. (1994).

4. RESULTS

Table 1 Cosmic dose rates

Table 2 Water contents, radionuclide contents

Table 3 a- Values, equivalent doses, dose rates and luminescence ages

Table 1: Cosmic Dose Rates

Laboratory Code	Depth Below the Surface(m)	Cosmic Dose Rate (Gy/ka)	Field Code
WLL1211	3.35	0.1331±0.0067	T16-01-OSL B
WLL1212	0.75	0.1884±0.0094	T16-01-OSL G
WLL1213	2.95	0.1401±0.0070	T16-02-OSL A
WLL1214	0.70	0.1897±0.0095	T16-02-OSL E
WLL1215	1.50	0.1699±0.0085	T16-03-OSL A
WLL1216	2.00	0.1588±0.0079	T16-03-OSL D
WLL1217	0.95	0.1832±0.0092	T16-03-OSL G

Table 2: Water Contents, Radionuclide Contents

Laboratory Code	Water Content (%)	U(ppm) from ^{234}Th	U(ppm) from ^{226}Ra, ^{214}Pb, ^{214}Bi	U(ppm) from ^{210}Pb	Th(ppm) From ^{208}Tl ^{212}Pb ^{228}Ac	K(%)	Field Code
WLL1211	14.2	2.84±0.19	2.72±0.11	2.67±0.15	9.01±0.10	1.74±0.03	T16-01-OSL B
WLL1212	14.2	2.89±0.19	2.84±0.12	2.55±0.15	10.31±0.11	1.34±0.03	T16-01-OSL G
WLL1213	28.1	3.77±0.25	4.15±0.16	4.51±0.22	23.26±0.22	2.51±0.05	T16-02-OSL A
WLL1214	14.6	2.67±0.18	2.70±0.12	2.70±0.15	9.33±0.10	1.30±0.03	T16-02-OSL E
WLL1215	15.6	3.18±0.20	2.85±0.12	2.59±0.15	11.07±0.12	1.81±0.04	T16-03-OSL A
WLL1216	17.1	2.79±0.19	2.63±0.12	2.66±0.15	10.16±0.11	1.31±0.03	T16-03-OSL D
WLL1217	13.2	3.28±0.21	3.20±0.13	3.12±0.17	11.59±0.12	1.35±0.03	T16-03-OSL G

8

Table 3 a- Values, equivalent doses, dose rates and luminescence ages

Laboratory Code	a-value	D_e(Gy)	Dose Rate(Gy/ka)	**Luminescence Age(ka)**	Field Code
WLL1211	0.05±0.01	168.88±36.32 123.21±2.61(SAR)	3.38±0.11	**50.0±10.9** **36.5±1.4(SAR)**	T16-01-OSL B
WLL1212	0.09±0.02	41.76±2.85	3.65±0.13	**11.4±0.9**	T16-01-OSL G
WLL1213	0.03±0.01	358.52±43.18 336.09±10.79(SAR)	4.76±0.18	**75.3±9.5** **70.6±3.5(SAR)**	T16-02-OSL A
WLL1214	0.07±0.01	64.83±5.16	3.24±0.12	**20.0±1.7**	T16-02-OSL E
WLL1215	0.07±0.02	162.4±13.53	3.87±0.23	**42.0±4.3**	T16-03-OSL A
WLL1216	0.08±0.01	95.61±5.31	3.25±0.12	**29.4±1.9**	T16-03-OSL D
WLL1217	0.06±0.004	60.52±3.71 60.53±0.79(SAR)	3.62±0.08	**16.7±1.1** **16.7±0.4(SAR)**	T16-03-OSL G

5. REFERENCES

Guérin, G., Mercier, N., Adamiec, G. 2011: Dose- rate conversion factors: update. Ancient TL, Vol.29, No.1, 5-8.

Murray, A.S. & Wintle, A.G. 2000: Luminescence dating of quartz using an improved single aliquot regenerative dose protocol. Radiation Measurements 32, 57-73.

Prescott, J.R. & Hutton, J.T. 1994: Cosmic ray contributions to dose rates for luminescence and ESR dating: Large depths and long-term time variations. Radiation Measurements. Vol.23,Nos.2/3, 497-500.

APPENDIX 2 RADIOCARBON DATING REPORT

Rafter Radiocarbon

Accelerator Mass Spectrometry Result

This result for the sample submitted is for the exclusive use of the submitter. All liability whatsoever to any third party is excluded.

NZA 62203
R 40940/2
Job No: 205616
Report issued: 28 Nov 2016

Sample ID	Titri T16-02 14CB(b2)
Description	Organic silt
Fraction dated	Sediment
Submitter	Marcus Vandergoes GNS Science

Conventional Radiocarbon Age (years BP)	**Background**	±		
$\delta^{13}C$ (‰) and type of measurement	-28.8	±	0.2	IRMS
Fraction modern	0.0044	±	0.0016	
$\Delta^{14}C$ (‰) and collection date	-995.6	±	1.6	17 Feb 2016

Measurement Comment: Slightly small sample, but treated as regular size since it is background (i.e. no special corrections).
This result is indistinguishable from 14C-free background materials prepared and measured concurrently with this sample. Therefore the reported fraction modern is a limiting age, not absolute.

Sample Treatment Details

Description of sample when received: sample submitted wrapped in plastic wrap as a large piece of damp sediment that was composed of many layers alternating between Munsell chart 2.5 5/2 grey brown and 4/1 dark grey. Under the microscope the sample was broken apart with a scalpel to look macrofossils. The darker layers seemed to have a lot of fine organics in matrix. Some root hairs were observed but no macro fossils. Sample prepared by: Wet Sieve. Pretreatment description: began sieving to 90 micron. Occasional dark coloured organic material that was strong enough to be lifted off the screen was isolated. A few very small plant flakes were also isolated along with black seed, stored separately. Talked to submitters and seeds, probably from grasses or sedge, were isolated through sieving, until enough mass was collected for treatment. Sample checked under microscope by Marcus before treatment. Root hairs removed and sample transferred to tube for treatment. Reed materials and degraded wood was also stored as backup material. Chemical pretreatment was by acid, alkali, (which was repeated), acid. Weight obtained after chemical pretreatment was 0.8mg. Carbon dioxide was generated by elemental analyser combustion and 0.3mgC was obtained. Sample carbon dioxide was converted to graphite by reduction with hydrogen over iron catalyst.

Conventional Radiocarbon Age and $\Delta^{14}C$ are reported as defined by Stuiver and Polach (*Radiocarbon 19*:355-363, 1977). $\Delta^{14}C$ is reported only if collection date was supplied and is decay corrected to that date. Fraction modern (F) is the blank corrected fraction modern normalized to $\delta^{13}C$ of -25‰, defined by Donahue et al. (*Radiocarbon, 32*(2):135-142, 1990). $\delta^{13}C$ normalization is always performed using $\delta^{13}C$ measured by AMS, thus accounting for AMS fractionation. Although not used in the ^{14}C calculations, the environmental $\delta^{13}C$ measured offline by IRMS is reported if sufficient sample material was available. The reported errors comprise statistical errors in sample and standard determinations, combined in quadrature with a system error based on the analysis of an ongoing series of measurements of standard materials. Further details of pretreatment and analysis are available on request.

National Isotope Centre, GNS Science
PO Box 31-312 Lower Hutt, New Zealand Phone +64 4 570 4644
Email radiocarbon@gns.cri.nz Website www.RafterRadiocarbon.co.nz

www.gns.cri.nz

Principal Location

1 Fairway Drive, Avalon
Lower Hutt 5010
PO Box 30368
Lower Hutt 5040
New Zealand
T +64-4-570 1444
F +64-4-570 4600

Other Locations

Dunedin Research Centre
764 Cumberland Street
Private Bag 1930
Dunedin 9054
New Zealand
T +64-3-477 4050
F +64-3-477 5232

Wairakei Research Centre
114 Karetoto Road
Private Bag 2000
Taupo 3352
New Zealand
T +64-7-374 8211
F +64-7-374 8199

National Isotope Centre
30 Gracefield Road
PO Box 30368
Lower Hutt 5040
New Zealand
T +64-4-570 1444
F +64-4-570 4657